WELL STRATEGIES FOR ENHANCED TIGHT OIL RECOVERY

A Thesis

Presented to

the Faculty of the Department of Petroleum Engineering

University of Houston

In Partial Fulfillment

of the Requirements for the Degree

Master of Science

in Petroleum Engineering

by

Daniil Ariskin

August 2016

WELL STRATEGIES FOR ENHANCED TIGHT OIL RECOVERY

Daniil Ariskin

Approved:

Chair of the Committee
Christine Ehlig-Economides,
Professor, Petroleum
Engineering

Committee Members:

Ali Daneshy, Adjunct Professor,
Petroleum Engineering

Guan Qin, Associate Professor,
Petroleum Engineering

Suresh K. Khator, Associate Dean,
Cullen College of Engineering

Mohamed Y. Soliman, Professor
and Chair of Department in
Petroleum Engineering

ACKNOWLEDGEMENTS

I would like to express my sincere appreciation to my committee chair, Dr. Christine Ehlig-Economides, for her invaluable guidance and profound knowledge in the research topic as well as to my committee members Dr. Ali Daneshy and Dr. Guan Qin for theirs input over the course of this work.

In addition, I would like to thank the Petroleum Engineering department faculty and staff for enriching my academic and professional knowledge during my time at the University of Houston.

Finally, I would like to thank my lovely wife Valentina for her love, care, understanding, and patience. That part of my life would not be possible without her support.

WELL STRATEGIES FOR ENHANCED TIGHT OIL RECOVERY

An Abstract

of a

Thesis

Presented to

the Faculty of the Department of Petroleum Engineering

University of Houston

In Partial Fulfillment

of the Requirements for the Degree

Master of Science

in Petroleum Engineering

by

Daniil Ariskin

August 2016

ABSTRACT

The worldwide technically recoverable tight oil resources estimated to be 418.9 billion barrels, and about 78.2 billion are located in the US. Despite the yearly increase in oil production from the unconventional formations, the operator companies were concentrating theirs effort on the improving stimulation techniques rather than production techniques and increasing the recovery factor.

Waterflooding is the most economical and wildly used enhanced oil recovery approach. So far, the attempts to implement waterflood in tight oil reservoirs have not been successful, and many operators do not see it as a technically and economically viable option.

Multiple fracture horizontal wells (MFHW) have proven to be very successful for primary development of tight oil reservoirs. This research analyzed why the use of existing MFHWs for waterflooding has failed. Then, we investigated more favorable MFHW patterns designed from the beginning for secondary oil recovery. Analytical modeling was used to evaluate wells specifically designed to benefit from plane-to-plane waterflooding. Based on that, we have proposed a new well pattern design strategy for implementing waterflood in the tight oil formations.

TABLE OF CONTENTS

LIST OF FIGURES

LIST OF TABLES

NOMENCLATURE

μ_o	=	Oil-phase viscosity, cp
μ_{ob}	=	Oil viscosity at bubble point pressure, cp
μ_{od}	=	Dead oil viscosity, cp
μ_w	=	Water-phase viscosity, cp
A	=	Cross-sectional flow area, ft^2
A_w	=	Drainage surface area of the well, ac
B_o	=	Oil formation volume factor (FVF), bbl/STB
B_{ob}	=	Oil formation volume factor (FVF) at bubble point pressure, bbl/STB
B_w	=	Water formation volume factor (FVF), bbl/STB
C_{fD}	=	Dimensionless infinite fracture conductivity
c_o	=	Oil isothermal compressibility, psi^{-1}
C_{prop}	=	Proppant cost, $/lbm
C_{pump}	=	Pumping charges, $/fracture
C_{wh}	=	Horizontal well construction cost, $/ft
C_{wv}	=	Vertical well construction cost, $/ft
D_{pmax}	=	Max proppant diameter, inch
f_o	=	Volume fraction of oil phase, fraction
f_w	=	Volume fraction of water phase, fraction
f_{wf}	=	Fractional flow of water at breakthrough, fraction
g	=	Acceleration of gravity, ft/s

γ_{gp} = Gas specific gravity at separator conditions

γ_{gs} = Gas specific gravity at separator conditions of 100 psig

γ_{oIPA} = Oil gravity, ° API

H = Reservoir depth, ft

h_f = Hydraulic fracture height, ft

i = Discount rate, fraction

k = Reservoir permeability, md

k_f = Proppant pack permeability, md

k_o = Permeability to oil, md

k_{ro} = Oil relative permeability, fraction

$k_{ro}(S_{wc})$ = Oil relative permeability at connate water saturation, fraction

k_{rw} = Water relative permeability, fraction

$k_{rw}(S_{or})$ = Water relative permeability at residual oil saturation, fraction

k_w = Permeability to water, md

L = Well spacing, ft

L_w = Length of the horizontal section of the well, ft

n_o = Oil Corey exponent

n_w = Water Corey exponent

ϕ = Reservoir porosity, fraction

ϕ_f = Porosity of proppant pack, fraction

p = Reservoir pressure, psi

P = Crude oil market price, $/STB

p_{bp} = Bubble point pressure, psi

p_i = Initial reservoir pressure, psi

p_{inj} = Injection pressure, psi

p_{injs} = Injection pressure safety factor, psi

p_p = Pressure at producing well, psi

p_{sep} = Separator pressure, psia

q_o = Oil volumetric flow rates, bbl/day

q_t = Total volumetric flow rates, bbl/day

q_w = Water volumetric flow rates, bbl/day

r = Annual discount rate, fraction

R_s = Solution GOR, scf/STB

R_t = Net cash flow, $

S = Water salinity, wt. %

S_{or} = Residual oil saturation, fraction

S_w = Water saturation, fraction

S_{wbt} = Average water saturation at breakthrough, fraction

S_{wc} = Connate water saturation, fraction

S_{wf} = Water saturation at breakthrough, fraction

t = Time, hr

T = Reservoir temperature, F

T_{sep} = Separator temperature, F

v = Poisson's ration, fraction

w	=	Fracture width, inch
x	=	Distance coordinate in the linear system, ft
x_f	=	Half hydraulic fracture length, ft
x_s	=	Hydraulic fracture spacing, ft
$x_{s(I\text{-}P)}$	=	Distance between I-P fractures, ft
α	=	Biot's poroelastic constant, fraction
$\Delta p_{I\text{-}P}$	=	Injector-Producer pressure drop, psi
λ_r^{-1}	=	Apparent viscosity, cp
λ_{ro}	=	Oil relative mobility, cp^{-1}
λ_{rw}	=	Water relative mobility, cp^{-1}
ρ	=	Rock density, lb/ft^3
ρ_{prop}	=	Specific gravity of proppant material
σ_h	=	Horizontal stress, psi
σ_{hmin}	=	Absolute minimum horizontal stress, psi
σ_v	=	Vertical stress, psi

CHAPTER 1 INTRODUCTION

The US Energy Information Administration in its World Shale Resource Assessments (EIA 2013, 2015a) estimated worldwide technically recoverable tight oil resources to be 418.9 billion barrels, and about 78.2 billion are located in the US. Annual Energy Outlook 2015 (EIA 2015b) expects the daily shale oil production to increase from 3.15 million barrels in 2013 to the 5.6 million barrels by 2020 that is almost 80% increase and more than 50% of the total US projected oil production. This outlook shows the significance of the shale oil resources for the US economy and the importance of research in that area.

A strategically designed well pattern of multiple transverse fracture horizontal wells can be a key part of successful waterflood program. It could deliver an additional oil production and significantly improve recovery factor of tight oil formations.

This chapter provides a problem description, explains the study objective, outlines the approach we have taken, and indicates how the thesis is organized.

1.1 Problem description

The success of the multi-traverse fractured horizontal well technology has enabled extensive oil production from tight formations during the last decade (Miller et al., 2008, Rankin 2010). However, wells and well patterns, generally, have been drilled with one goal: to cover the leased acreage and assure immediate primary production. Subsequent infill drilling programs usually increased reservoir stimulated area by stimulating undrained areas between wells but not enhancing oil recovery (Foster 2014). Typical

recovery factor for the tight reservoirs usually is in the range of 5 – 10% (Jacobs 2016, Foster 2014), that means that by increasing recovery factor to 10 – 20% will double the US oil production from tight reservoirs.

Waterflooding is an economical and wildly used enhanced oil recovery approach. So far, the attempts to implement waterflood in tight oil reservoirs were not very successful, and many operators do not see it as a technically and economically viable option. .

1.2 Study objectives

The purpose of this study was to design and evaluate a well pattern using MTFHWs that can optimize waterflood recovery of tight oil. We then quantified the benefits of proposed well pattern design using available analytical methods and assessed its applicability in the major US shale plays.

1.3 Approach

We designed a waterflood pattern using laterally parallel horizontal wells drilled at an angle of at least 45° with the direction of maximum lateral field stress. Transverse fractures created along the length of the horizontal wells are to be positioned strategically so that injection and production well fractures alternate. The configuration produces the most efficient “plane to plane” waterflood performance between each pair of injection and production fracture planes.

We then developed an analytical screening tool for assessing the waterflood performance of designed well patterns with different well spacing, fracture spacing, and reservoir and fluid properties. Finally, we used the screening tool to check the applicability of the designed pattern to the major US shale plays based on publically available reservoir data.

1.4 Organization of the thesis

This thesis consists of five chapters. This section will briefly describe the content of each of them.

Chapter 1: Introduction – this chapter provides information about problem description, study objectives, approach to the problem, and organization of the thesis.

Chapter 2: Literature review - this chapter provides a brief review of historical aspects of waterflood application, waterflood fundamentals, the background of development and application of multiple transverse fracture horizontal wells for gas and oil production in tight formations, basics of field stresses and its estimation approach. This chapter also reviews publicly available information on implementing waterflood in a tight reservoir.

Chapter 3: Development of well pattern – this chapter describes design of widely used MTFHW patterns and why they are not well suited to secondary waterflood displacement. We then show an alternative well pattern and explain development of analytical screening tool to evaluate which formations may be candidates for waterflooding with this pattern.

Chapter 4: Well pattern application and sensitivity – this chapter uses the analytical tool developed in Chapter 3 to investigate the applicability of the pattern to the different pattern geometries and key reservoir properties. We apply the screening program to the major US tight oil plays and conclude whether a given formation is a candidate for waterflooding with this well pattern design.

Chapter 5: Conclusions and recommendations – this chapter summarizes the findings and concludes the developed ideas in this thesis. Recommendations for the future work in this area of research are also provided.

Appendices: Appendix A shows the input screen of the analytical screening tool. Appendix B shows equations and correlations used for default values based on required inputs. Appendix C and Appendix D represent the equations to assess the performance of the linear waterflood at constant pressure drop and constant injection rate accordingly.

CHAPTER 2 LITERATURE REVIEW

This chapter will summarize the key points of prior work relevant to this study, including historical development of the conventional waterflood and its fundamentals, theory and adaptation of the multiple transverse fracture horizontal wells (MTFHW), field stresses and their effect on the hydraulic fractures orientation, and review of the research studies and field trials associated with waterflooding in tight oil formations.

2.1 Rationale for waterflooding

Hayes (1974) determined enhanced oil recovery (EOR) as any method used to recover more oil from a reservoir than would be produced by primary recovery. The natural reservoir energy is the main driver for displacing oil to the production wells during primary production. Traditionally, EOR supplies extra energy to the reservoir by injecting a fluid (gas or liquid) into the reservoir.

Willhite (1986) pointed out that waterflooding is the most widely applied EOR process, and its benefits were discovered as early as at the end of the 19th century and associated with the development of Bradford field in Pennsylvania. Figure 1.1 (from Willhite 1986) shows the production history of the Bradford field for more than 100 years of producing life. The effects of waterflooding on production from this field are tremendous. By early 1930's the water-injection operations started in Oklahoma, Kansas, and Texas. Nevertheless, wider popularity in the US and worldwide of the waterflooding technique occurred in the late 1940's and early 1950's.

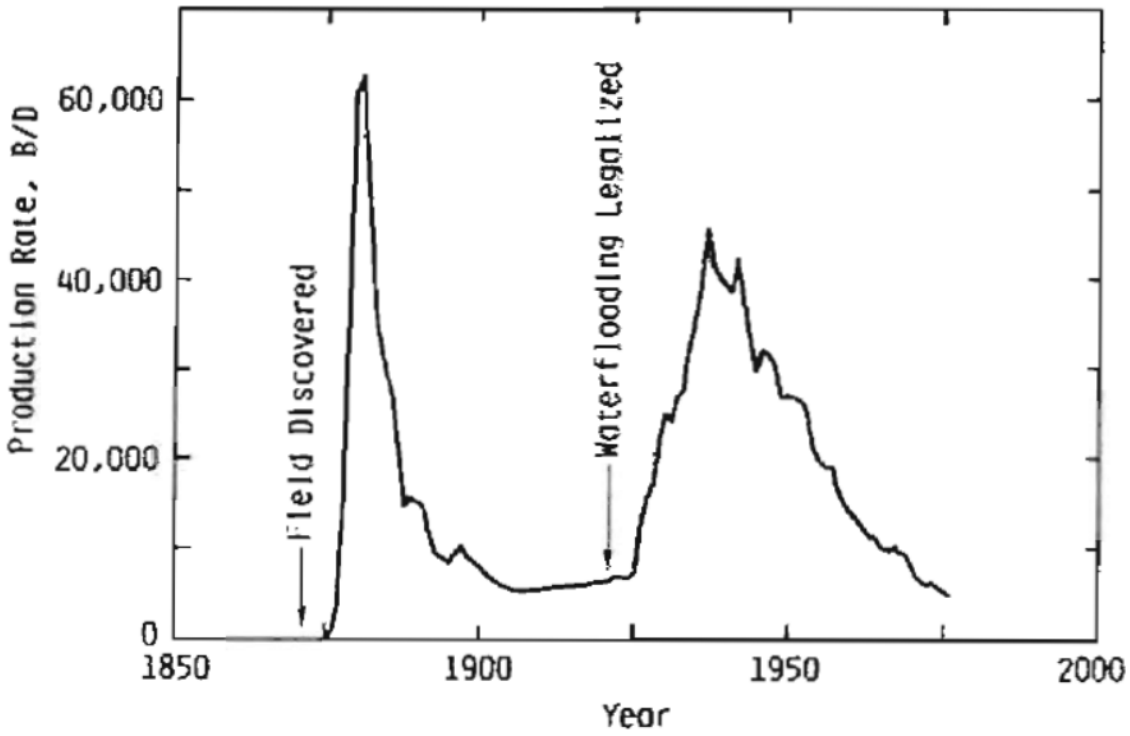

Figure 2.1. Production history of the Bradford field.

2.2 Waterflood fundamentals

Buckley and Leverett (1942) introduced a model that describes the displacement of oil by water in the linear flow system by application of the law of conservation of mass to the flow of two fluids (oil and water). They based this model on the following three assumptions: incompressible flow, fractional flow of water is a function only of the water saturation, and no mass transfer between phases. Buckley and Leverett pointed out an important concept of a fractional flow. The fractional flow of a phase, *f*, is defined as the volume fraction of the phase that is flowing at position *x* in the linear system at the time *t*. For oil and water phases,

$$f_o = \frac{q_o}{q_t} = \frac{q_o}{q_w + q_o} \tag{2.1}$$

and

$$f_w = \frac{q_w}{q_t} = \frac{q_w}{q_w + q_o}, \tag{2.2}$$

where q_w and q_o – water and oil volumetric flow rates, q_t – total volumetric flow rate. Because the fractional flow is a volume balance,

$$f_o + f_w = 1. \tag{2.3}$$

Equation (2.2) could be written in another form using permeability to water and oil (k_w, k_o) as well as water-phase and oil-phase viscosities (μ_w, μ_o)

$$f_w = \frac{1}{1 + \left(\frac{k_o}{k_w}\right)\left(\frac{\mu_w}{\mu_o}\right)}. \tag{2.4}$$

If we plot fractional flow of water (equations (2.2) or (2.4)) versus water saturation (S_w) the resultant plot is called fractional flow curve and shown in Figure 2.2 (Craig 1971).

Terwilliger et al. (1951) studied the application of Buckley-Leverett model and confirmed its validity by experiments. In addition, the authors developed the concept of the stabilized and non-stabilized zones and showed that by laying a tangent to the fractional flow curve the saturation at the upstream end of the stabilized zone could be defined as shown in Figure 2.3 (Willhite 1986).

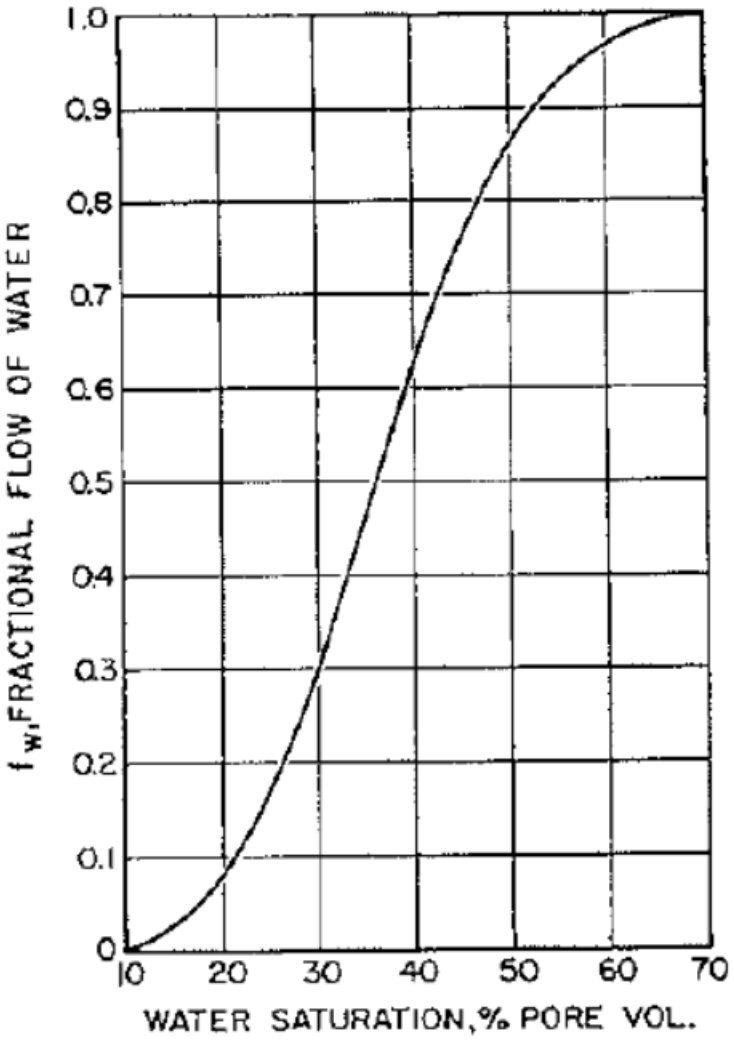

Figure 2.2. Fractional flow curve.

Welge (1952) showed that construction of a tangent to the fractional flow curve was equivalent to the "balancing of areas" technique suggested by Buckley and Leverett. Welge derived an equation that relates the average water saturation (hence the total oil recovery), the cumulative injected water volume and fraction of oil flowing at the outflow end of the system (hence water cut).

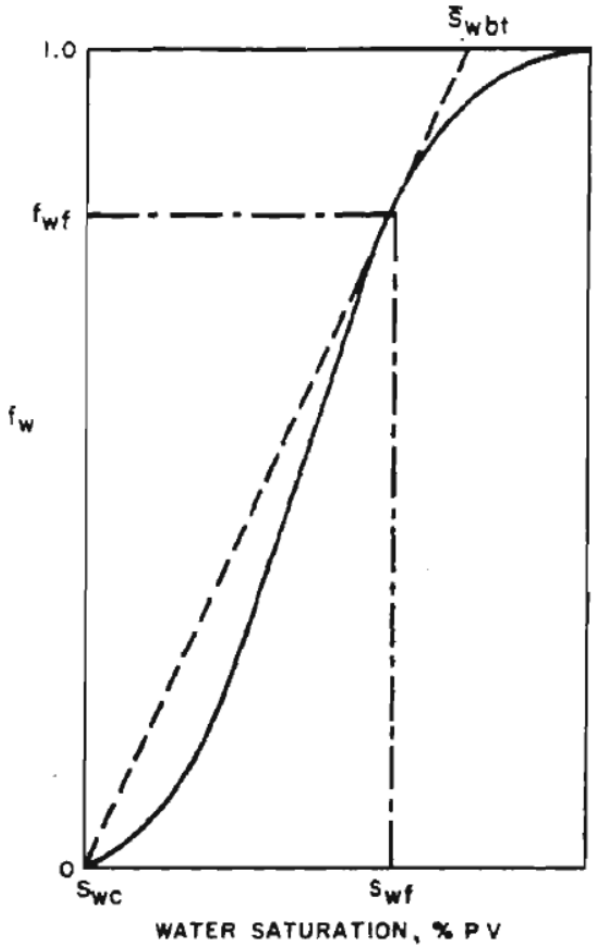

Figure 2.3. Determination of flood front saturation by laying tangent to the f_w curve.

Wolcott (2009) stated in his Applied Waterflooding book that the Buckley-Leverett technique is the fundamental basis for waterflooding that governs all the calculations in the subject whether performed using analytical or numerical simulation techniques. The analytical approach is the quickest one and tends to overestimate the efficiency of waterflooding because it cannot account for significant changes in reservoir properties or saturations across the areal or vertical extent of the reservoir or when crossflow or gravity segregation are important. In addition, reservoir simulation technique is able to account for rock and fluid compressibility (Whillhite 1986).

2.3 Multiple transverse fracture horizontal wells (MTFHW)

A number of investigators have addressed the performance and application for primary production of the horizontal wells intersected by multiple transverse vertical fractures in the past. Maersk Oil accomplished one of the first successful application of MTFHW in tight chalk oil reservoirs of North See in 1987 (Andersen, Hansen and Fjeldgaard 1988). They reported that of a total of 41 wells producing from Dan field, some 25% of total production was coming from the 3 multi-fractured horizontal well completions. The actual section of the one of the Dan's MTFHWs and fractures locations is shown in Figure 2.4. According to Tehrani (1992), the permeability of Dan field is in the range from 0.1 to 1 md.

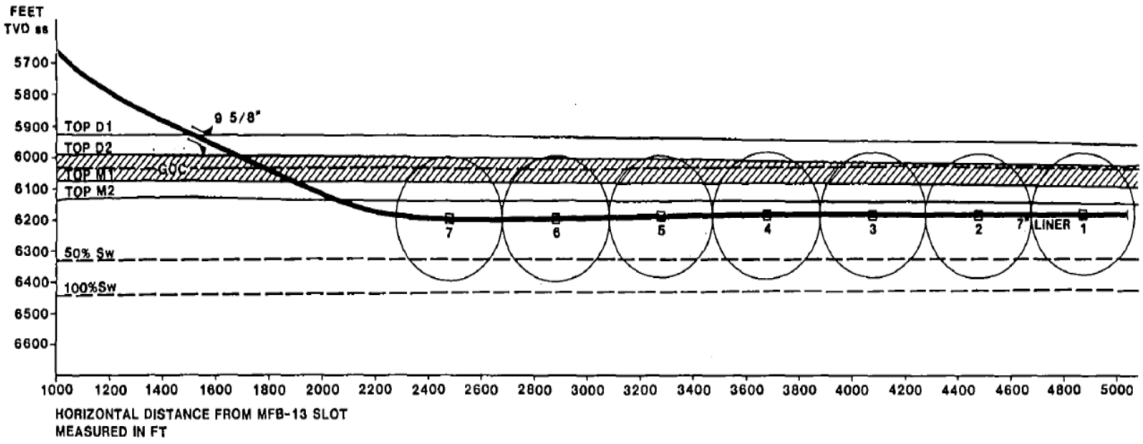

Figure 2.4. The lower section of MFB-13 well and fractures locations.

Yost and Overby (1989) reported the application of MTFHW in a gas formation of Devoian shale of Appalachian Basin with an average permeability of 0.2 md. They indicated that both long horizontal drilling and multiple stimulations are required to achieve high folds of increase in production compared to conventional vertical wells.

Mukherjee and Economides (1991) presented the results of a parametric study of the performance of vertical and horizontal fractured wells, including a technique for estimating the optimum number of transverse fractures in horizontal wells.

In recent years of widespread development of unconventional resources, the application of MTFHWs in gas production was initially reported in Australia by Crosby et al. (1998) for reservoir formations with a permeability below 0.1 md. As part of his paper, he shows a comparison between the 10-year cumulative production estimations of various completion schemes with clear benefits of MTFHW completion (see Figure 2.5).

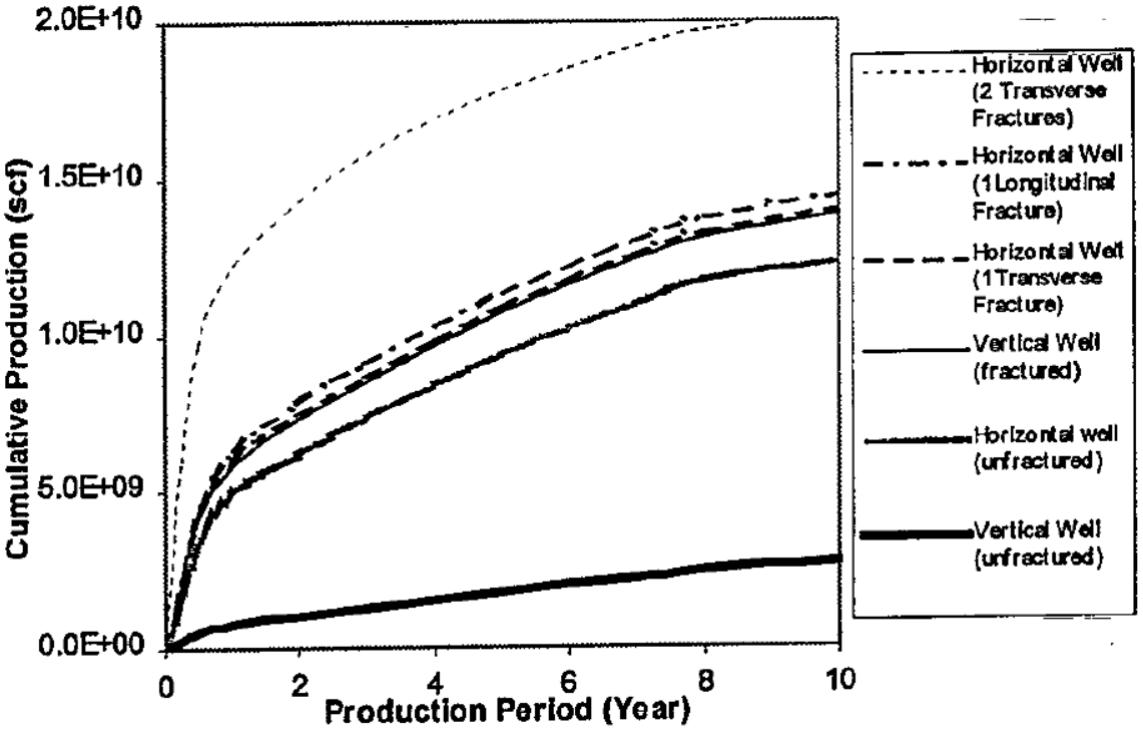

Figure 2.5. Comparisons of cumulative production for different well configurations.

In 2002 this well design was adopted in Barnett shale by Devon Energy (Bybee 2007) together with a slickwater fracture-stimulation approach developed by Mitchell Energy.

Typical permeability in the gas areas of Barnett shale is below 0.0005 md. After success in Barnett shale, the application of MTFHWs became a standard development technique of tight gas fields in the US (Arthur, Bohm and Layne 2008).

Eventually, Rankin (2010) reported that MTFHW approach had proved successful for the development of tight oil in Bakken formation with the average permeability of 0.04 md. He showed statistics of oil production per well versus the number of stages and quality of proppant reproduced in Figure 2.6. The higher the number of stages and quality of the proppant the better production results are expected. Forster (2014) noticed in his paper that MTFHW design typically supports only primary production with the recovery factor averaging about 5%.

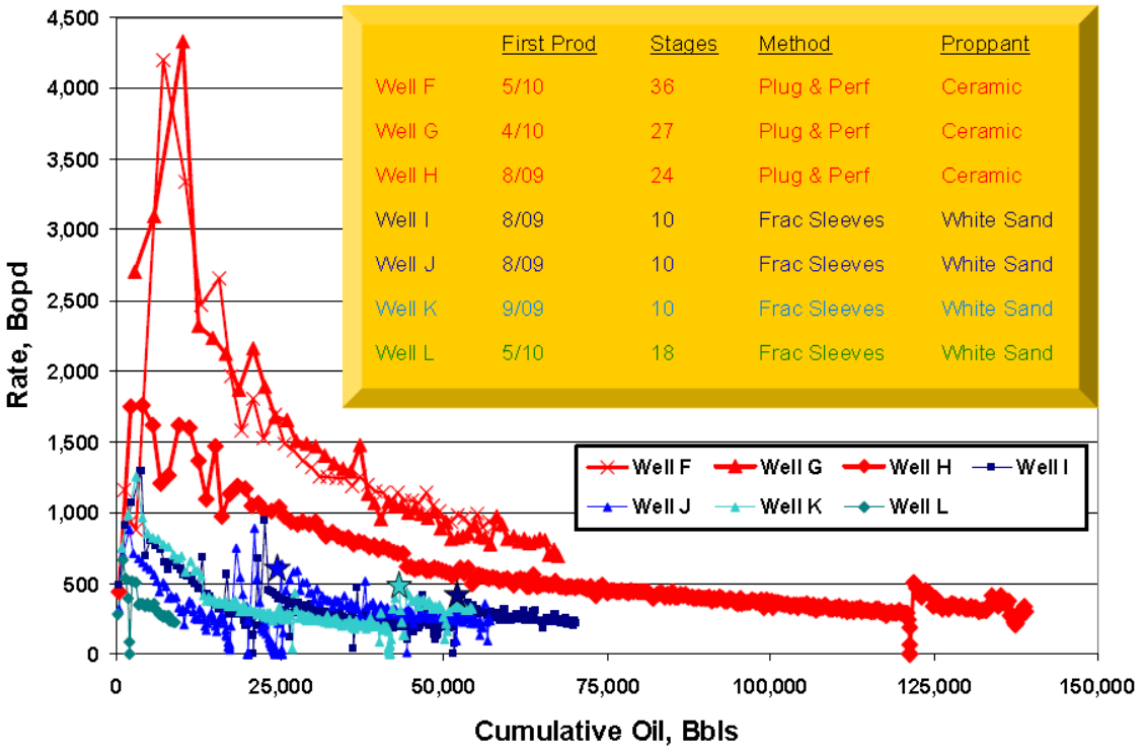

Figure 2.6. Production decline curves for well with a various number of stages.

2.4 Field stresses

Hubbert and Willis (1957) research showed that state of stress underground is not, in general, hydrostatic but depends on tectonic conditions. Generally, the least principal stress in the reservoirs is horizontal, and, because the hydraulically induced fractures form approximately perpendicular to the least principal stress, they should be vertical as shown in Figure 2.7. However, in the shallow or significantly overpressured reservoirs the least principal stress can be vertical, and in this rare case hydraulic fractures would be horizontal as shown in Figure 2.8.

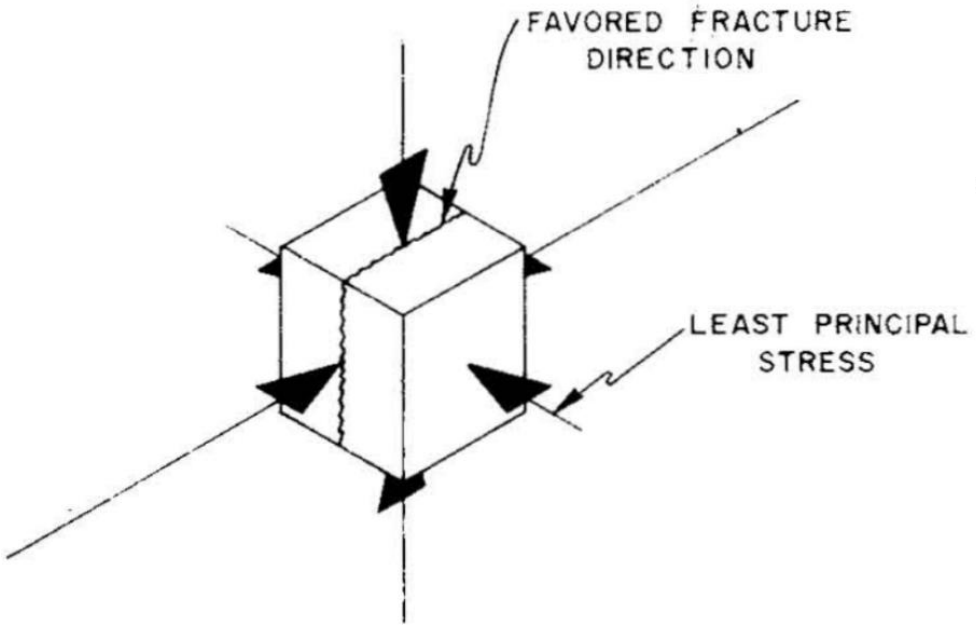

Figure 2.7. An example of vertical fracture development.

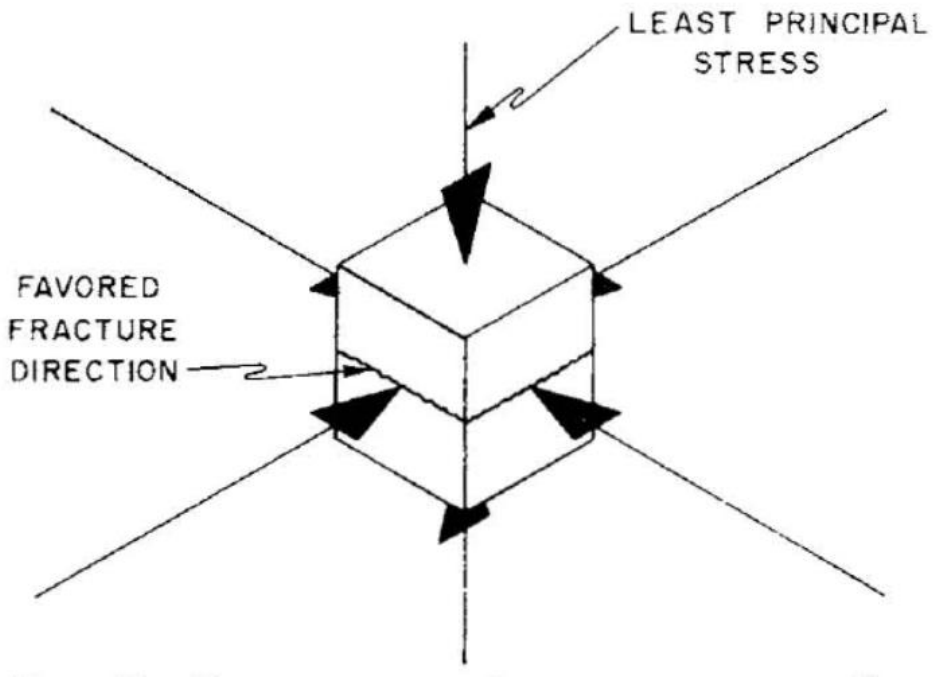

Figure 2.8. An example of horizontal fracture development.

The breakdown pressures are affected by the values of the pre-existing regional stresses, by the hole geometry including any pre existing fissures, and by the penetrating quality of the fluid. However, the minimum propagation pressures depend mainly on the magnitude of the least principal regional stress and are not significantly affected by the hole geometry or the penetrating quality of the fluid.

Soliman, Hunt, and El Rabaa (1990) provided a summary of some aspects of hydraulic fracturing of horizontal wells, including the conditions for the development of longitudinal or transverse vertical fractures.

Economides and Nolte (2000) made comprehensive research in the field of rock mechanics and reservoir stimulation through the fracturing. They pointed that stresses in the earth are functions of various parameters that include depth, lithology, pore pressure,

structure and tectonic setting. When the rock is under uniaxial strain conditions, the vertical stress is generated by the weight of the overburden rock and is the function of depth, density of the overlying rock and acceleration of gravity and could be calculated by the following formula

$$\sigma_v = \int_0^H \rho(H) g dH, \tag{2.5}$$

where ρ – the density of the overlying rock masses and g – the acceleration of gravity.

Then assuming the elasticity of the rock and using Biot's (1956) poroelastic constant the absolute horizontal stress could be calculated using the following formula

$$\sigma_h = \frac{\nu}{1-\nu}\sigma_v + p\alpha\frac{1-2\nu}{1-\nu}, \tag{2.6}$$

where ν – Poisson's ration, α – Biot's poroelastic constant, a p – reservoir pressure.

2.5 Waterflood in tight formations

Huang, Kaetzer and Bowlin (1996) reported one of the first attempts to implement a waterflood using a horizontal injection well in the New Hope Shallow Unit in 1991. The injection well was deemed unsuccessful due to injectivity issues shown in Figure 2.9. Estimated sandstone reservoir permeability range based on core plugs was from 0.04 to 10 md.

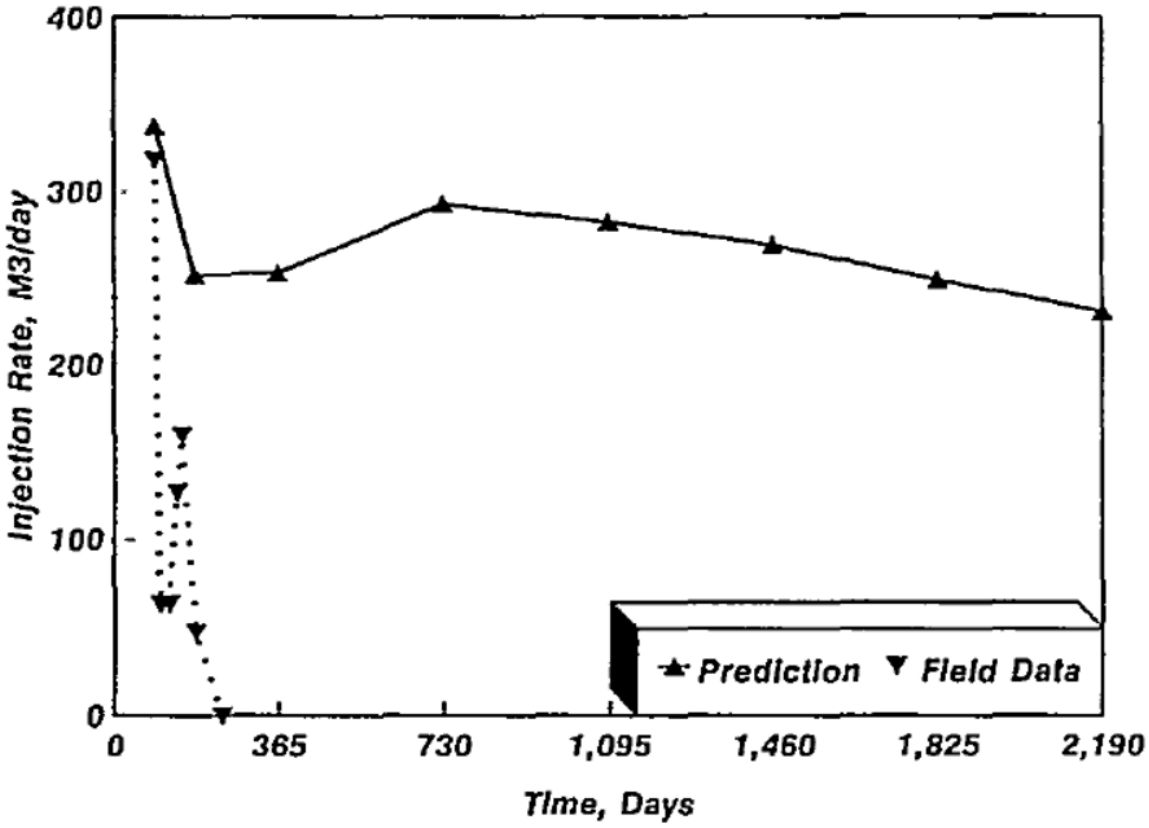

Figure 2.9. Horizontal well #70-2 water injection history.

Zwahlen and Patzek (1997) presented an analytical solution to estimate primary production in California diatomite fields (average permeability is about 0.1 md) developed by MTFHWs with the further conversion of some wells into water injectors. They estimated the effect of waterflood in the amount of 3% of OOIP which is about 30% of the primary production.

Sandhu (2011) modeled a Bakken waterflood case study, concluding that after 4 years of waterflooding the recovery factor would reach 10%, and that it would get to 32% in the 30-year production forecast. The model was based on the history matched simulation model with the reservoir permeability ranging from 0.5 to 5 md (Figure 2.10). He pointed out that due to low solution GOR, the reservoir pressure depletes very quickly, and water

injection is required early in the field life to compensate for that. The field pilot started in 2006 using four vertical injectors that later, due to injectivity issues were converted into horizontal wells. He indicated that waterflood is expected to bring on average an addition 50 – 100% of primary production and that the main limiting factors for the successful waterflood are matrix/fracture crossflow and reservoir heterogeneity. The wells in this study were not MTFHWs.

Based on a simulation study for a pilot waterflooding program for the Lower Shaunavon shale with the permeability in the range 0.05 – 0.6 md (shown in Figure 2.11), Thomas et al. (2014) voiced similar concerns regarding water breakthrough in producing fractures through the higher permeability streaks (up to 10 md) short-circuiting the effect of water injection.

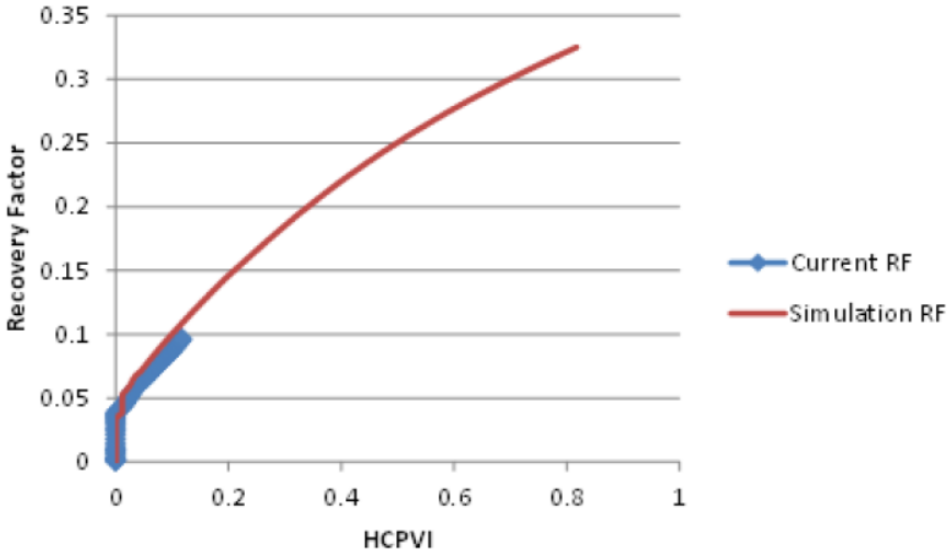

Figure 2.10. Recovery factor for Bakken case study.

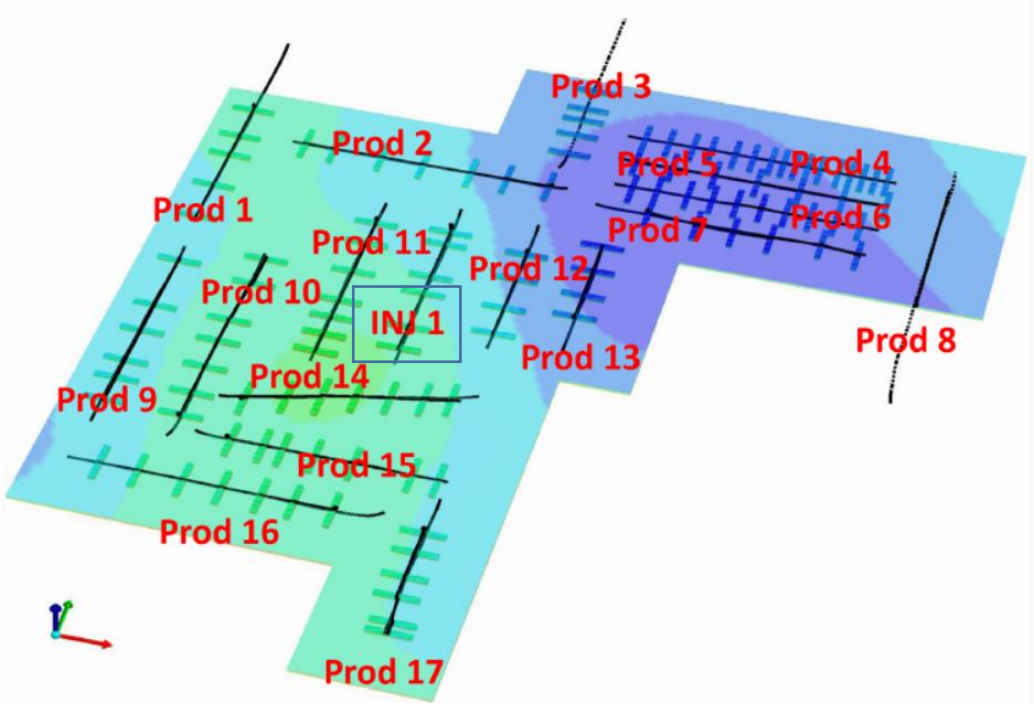

Figure 2.11. Top view of Lower Shaunavon pilot water injection area.

Morsy, Sheng, and Ezewu (2013) studied the potential of waterflood in the US shale formations using reservoir core and outcrops samples from Eagle Ford, Mancos, Barnett, and Marcellus and assessing their spontaneous imbibition characteristics. Figure 2.12 shows that the highest oil recovery of 59% was observed in the sample from Mancos.

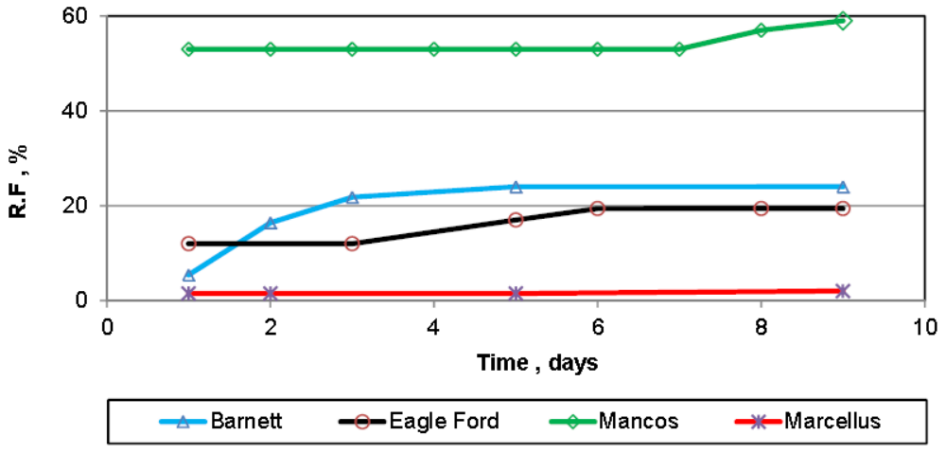

Figure 2.12. Recovery factor from spontaneous imbibition in fresh water.

Morsy, Sheng and Soliman (2013) studied the potential of waterflooding in Eagle Ford shale formation using sector model by simulating the area between two fractures (injecting and producing) of two MTFHWs as depicted in Figure 2.13. The permeability of the studied area was taking at 0.001 md. They indicated that recovery in the waterflood case could be improved by 30% in comparison with an only primary production case.

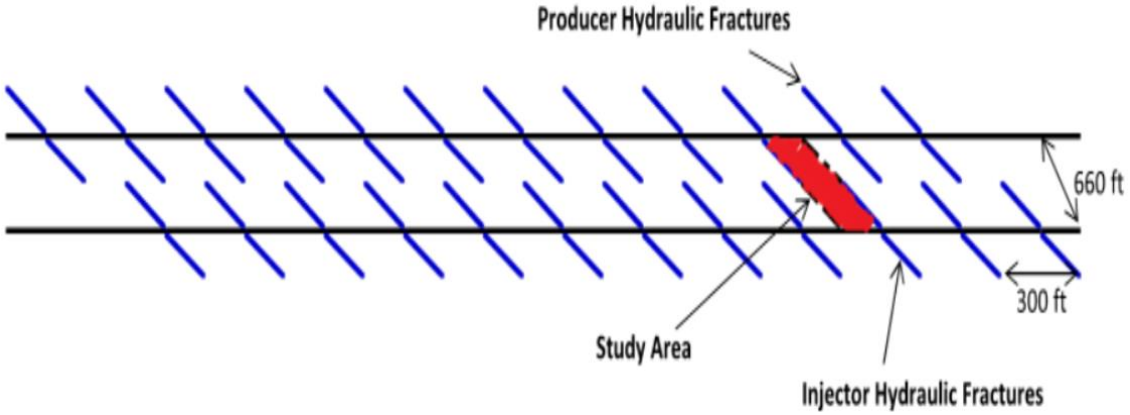

Figure 2.13. Schematic of two MTFHW and study area.

Hoffman and Evans (2016) published a summary of results from publicly available waterflood pilot programs in Bakken formation with permeability typically less than 0.1 md. The general locations of pilot programs are circled in Figure 2.14. The authors indicated that despite the fact that in some cases an increase in oil production was observed it might not be directly attributed to the waterflood performance. The small size of pilot programs, early water breakthrough due to short-circuiting and external factors such as frac-hits from nearby wells significantly obscured the conclusions that could be drawn from these pilot programs. On the other hand, these pilot programs proved that the injectivity in tight formations using MTFHWs does not appear to be an issue.

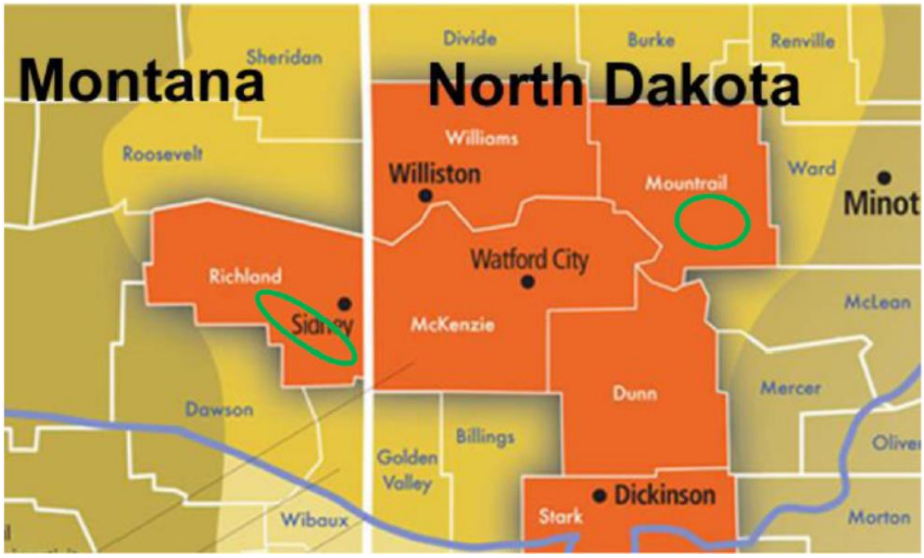

Figure 2.14. General locations of pilot tests in Bakken formation.

2.6 Chapter summary

This chapter has provided information on MTFHW theory and application. The theoretical basis for waterflood has been provided as well as the practical aspects of waterflood in the tight formation. Many authors have indicated the potential benefits of waterflood in the US shales as well as common pitfalls that preventing or limiting the benefits of the waterflood in the tight formations.

This theoretical and practical knowledge will be used in Chapter 3 to develop an optimized well pattern for water injection and quantify its performance.

CHAPTER 3 DEVELOPMENT OF WELL PATTERN

Chapter 2 indicates that report attempts to use existing MTFHWs for waterflooding have been largely unsuccessful. This chapter explains fundamental flaws in these attempts and introduces a different well pattern. We describe a screening tool developed for evaluating whether the fluid and formation properties of a given tight formation make it a candidate for the proposed well pattern.

3.1 Analysis of existing MTFHW patterns

The widely used well pattern for development and production from the tight formations consists of several horizontal wells drilled in the direction of least principal horizontal stress, each with a number of hydraulic fractures created along each horizontal section with fracture planes generally perpendicular to the wellbore, as shown in Figure 3.1.

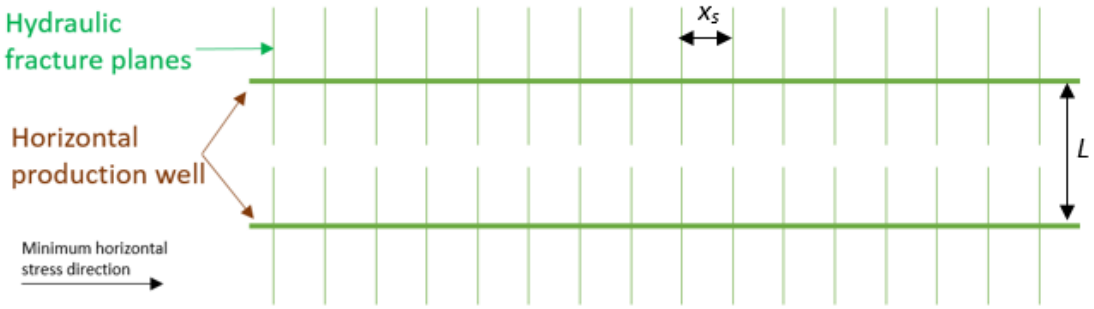

Figure 3.1. General MTFHW pattern.

The main design parameters for this general MTFHW pattern are well spacing (L) and fractures spacing (x_s). The lengths of the horizontal section (L_w) of the well is usually limited by drilling constraints, wellbore hydraulics or borders of the development area.

The most recent waterflood simulation and pilot programs reviewed in Chapter 2 were based on the similar well pattern design. After converting one of the wells into a water injector, the authors reported early breakthrough. Actually, such behavior should be expected.

Thomas et al. (2014) suggested that high permeability streaks caused early breakthrough. However, another likely reason may be the created fractures. Once on injection, both propped and/or secondary fractures in a MTFHW may open to flow and connect readily to propped and/or secondary fractures in surrounding production wells. The wealth of evidence that hydraulic fractures connect during the fracturing treatment (Lawal et al., 2013, Awada et al., 2016) indicates the likelihood of virtually instantaneous connection if the same wells are used for waterflooding. Figure 3.2 depicts water short circuiting through the closest fractures between injection and production wells and, hence, early water breakthrough and poor sweep efficiency.

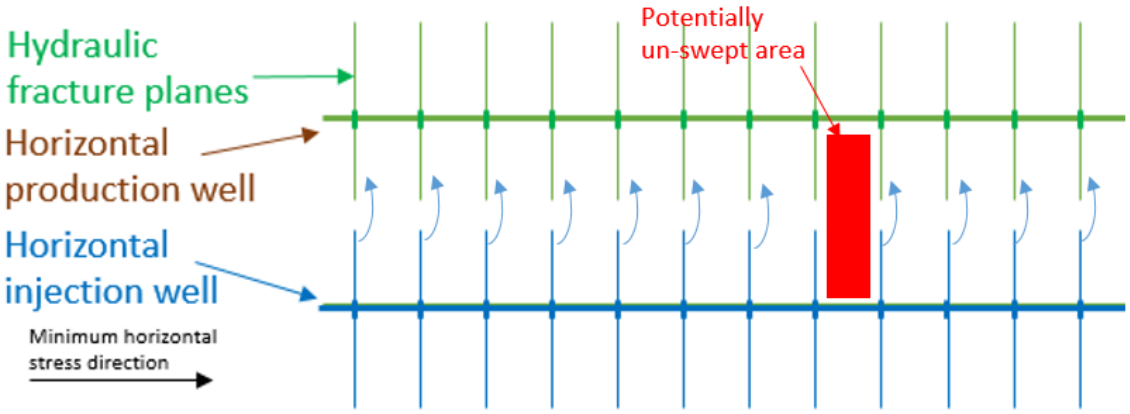

Figure 3.2. Conversion of general MTFHW pattern into water injection.

Another popular MTFHW pattern is based on creating fracture planes, induced from one horizontal well, in between of the other two fracture planes induced from the neighboring horizontal well. Figure 3.3 shows a modified zipper fracturing technique modeled by Morsy, Sheng and Soliman (2013).

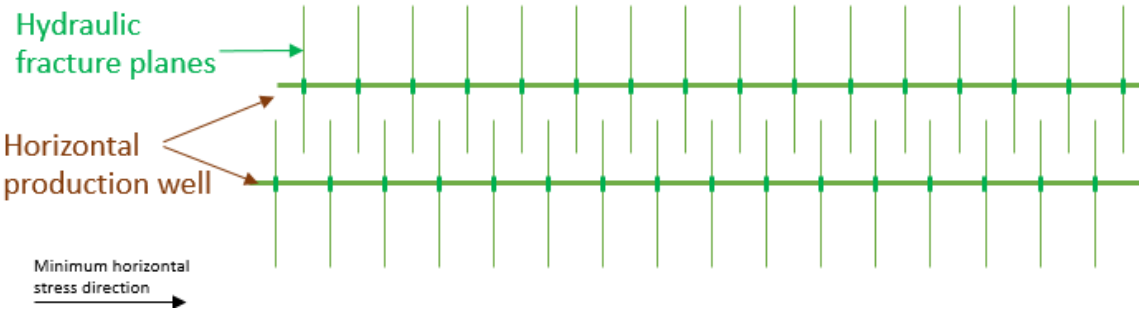

Figure 3.3. MTFHW pattern based on zipper-fracturing.

By converting one of the horizontal wells with zipper fracs into the water injector the waterflood becomes more efficient as shown in Figure 3.4. Unless the water injecting fracture plane goes all the way to the producing wellbore with poor cementing isolation, water has to flow linearly perpendicular to the producing fracture with a very efficient sweep in the area between injecting and producing fracture planes. This promising

approach is vastly superior to those reported previously. However, this requires considerable control on the placement of the fractures over the several hundred feet between wells. If any of the propped fractures intersect, they would likely short circuit the displacement between the wells. Also, half of the fracture planes are outside the well pattern.

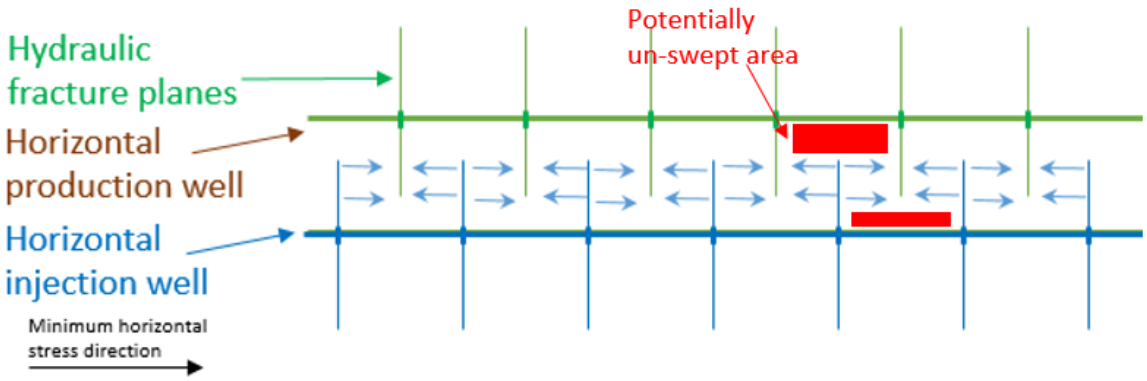

Figure 3.4. Conversion of zipper frac well into water injector.

3.2 Description of proposed well pattern

To mitigate or eliminate the disadvantages of the existing MTFHW patterns for secondary oil recovery described in the previous section, we developed a new design. The proposed pattern utilizes three laterally parallel horizontal wells drilled in the direction of minimum field stress. The central horizontal well is an injection well that is located between production wells. Transverse fractures are created along the length of the horizontal wells. Fractures for the injection well are positioned between fracture planes for the production wells and designed to be twice the length of the fractures of the production wells (Figure 3.5).

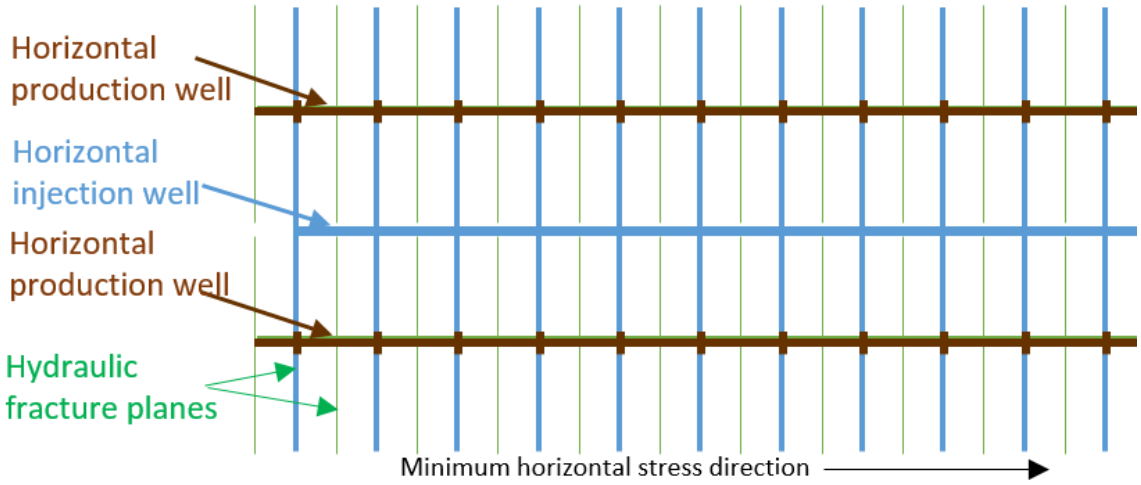

Figure 3.5. Design of the proposed MTFHW pattern.

Provided that the fracture planes of the injection well do not intersect with fracture planes of production wells, this configuration will produce the most efficient "plane-to-plane" waterflood performance between each injection and production fracture plane, as shown in Figure 3.6.

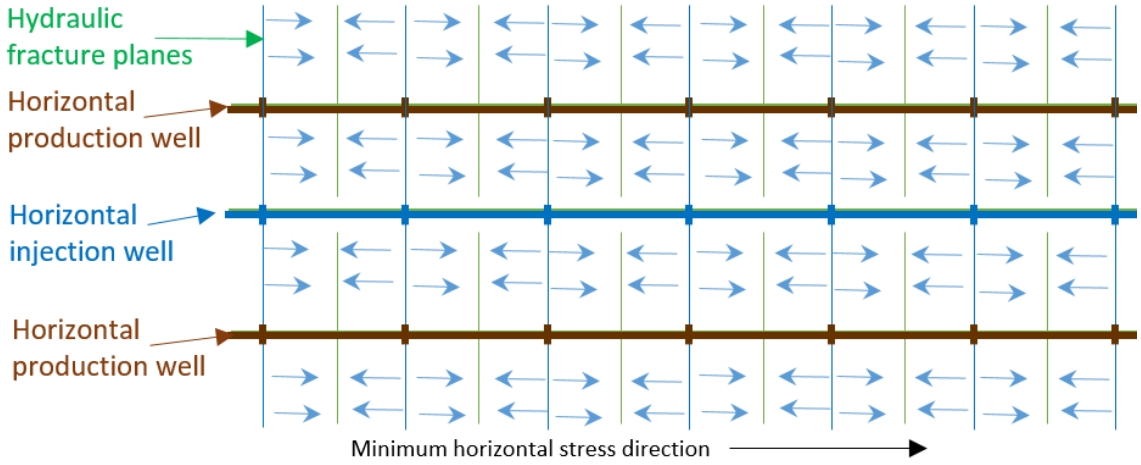

Figure 3.6. Performance of the proposed pattern during waterflood.

Before attempting to implement the proposed pattern the direction of the minimum principal horizontal field stress must be known. We propose to drill the water injection

well first, cement it and fracture with proppant with strategically selected fracture spacing that accounts for producing fractures that will go in between. Then drill two production wells and detect, while drilling, fractures created from the injection well.

Methods for detecting the fractures is a separate research topic. Plausible ways to detect the propped fractures include using tagged proppant, using a wellbore imaging tool, injecting into the injection well while drilling to enable detecting elevated pressure, and monitoring pressure in the injection well to detect intersection with each propped fracture.

With the known locations of the existing water injection fractures, each producing well should be properly cemented (shown by brown lines in Figures 3.5 and 3.6) to isolate its wellbore from these fractures and prevent crossflow along the completion. After that, the production fractures are created in between of existing water injection fractures. Producing fractures can connect with the producing fractures coming from another production well. Likewise, if the pattern is repeated, injecting fractures can connect with the injecting fractures in another injection well.

Pressure in the injection well should be monitored during fracturing of the production wells. A large pressure increase in the injection well would signal direct connection with the fracture(s) being injected at that time. After all of the fractures in production wells have been placed, production logs should be conducted along the production wells to identify direct fracture to fracture connection. Such connections should be sealed off before starting the waterflood.

The proposed design of MTFHW pattern requires a lot of information and technique to be implemented properly and perform optimally during waterflood. Proposing this design, we assume that the following construction assumptions are true. The fractures could be created in the intended location and their direction of propagation is perpendicular to the minimum horizontal field stress and could reach the designed length. The location of existing fractures could be detected while drilling and they could be properly isolated by cement. Injection well has a proper cementing bond that isolates it from the producing fractures if they cut through. Any inadvertent intersection between producing and injecting fracture planes has been plugged.

The proposed design results in plane to plane waterflood displacements between each pair of injection and production fractures. For n_f fractures from the injection well, this will be 4 n_f simultaneous plane to plane waterflood displacements. The next section explains the use of Buckley and Leverett 1942 theory to develop a first order screening tool for evaluating the profitability of this well pattern for given rock and fluid and economic parameters.

3.3 Description of analytical screening model

The Buckley and Leverett 1942 analytical model provides a straightforward basis for oil displacement calculations. Two versions of the screening tool were created: one for constant pressure drop between injecting and producing wells and one for constant injection rate. The following sections describe the inputs required for the analysis and illustrate results for a sample case.

The analytical screening tool model uses the following assumptions:

- incompressible fluids,
- immiscible two-phase oil and water flow,
- no capillary forces,
- homogeneous reservoir,
- no primary production (water injection starts from the beginning),
- infinite hydraulic fracture conductivity,
- maximum injection pressure limited by the value of minimum horizontal stress,
- economics governed by water breakthrough time or 3 years of production (whichever is earliest).

Table 3.1 shows the basic rock and fluid properties required for the model. These parameters are directly used in Buckley and Leverett calculations.

Table 3.1. Rock and fluid properties.

Rock and fluid properties	**Symbol**
Porosity, fraction	$\emptyset$
Permeability, md	k
Oil viscosity*, cp	μ_o
Water viscosity*, cp	μ_w
Water salinity, wt. %	S

*parameter can be estimated from required input values

The oil viscosity estimation is based on Vazuquez and Beggs (1980) and Beggs and Robinson (1975) correlations. The water viscosity estimation is based on McCain (1991) correlations and requires water salinity to be known (see Appendix B for details).

Required oil and water relative permeability input parameters are listed in Table 3.2.

Table 3.2. Relative permeability parameters.

Relative permeability	**Symbol**
Water Corey exponent	n_w
Oil Corey exponent	n_o
Connate water saturation, fraction	S_{wc}
Residual oil saturation, fraction	S_{or}
Water relative permeability at residual oil saturation, fraction	$k_{rw}(S_{or})$
Oil relative permeability at connate water saturation, fraction	$k_{ro}(S_{wc})$

Then Relative permeability of oil and water at different water saturations is calculated using Corey (1954) equations. For water relative permeability

$$k_{rw} = k_{rw}(S_{or}) \left(\frac{S_w - S_{wc}}{1 - S_{wc} - S_{or}} \right)^{n_w} \tag{3.1}$$

and for oil relative permeability

$$k_{ro} = k_{ro}(S_{wc}) \left(\frac{1 - S_w - S_{or}}{1 - S_{wc} - S_{or}} \right)^{n_o}. \tag{3.2}$$

The initial reservoir pressure, temperature, solution GOR, oil FVF, and bubble point pressure could be inputted directly or estimated based on the required input shown in Table 3.3.

Unless initial reservoir pressure is inputted directly, it assumed to be a hydrostatic pressure. The reservoir temperature is calculated based on geothermal coefficient unless it is provided directly. The bubble point pressure and solution GOR could be inputted directly or estimated based on Vazquez and Beggs (1980) correlations:

$$R_s = C_1 \gamma_{gs} p_{sep}^{C_2} \exp\left(C_3 \frac{\gamma_{oAPI}}{T + 460}\right) \tag{3.3}$$

and

$$P_{bp} = \left[\left(\frac{A_1 R_s}{\gamma_{gs}}\right) \text{antilog}\left(-A_3 \frac{\gamma_{oAPI}}{T + 460}\right)\right]^{A_2}, \tag{3.4}$$

where γ_{gs} – gas specific gravity that would result from separator condition of 100 psig and could be found as

$$\gamma_{gs} = \gamma_{gp}\left[1 + 5.912 \times 10^{-5} \gamma_{oAPI} T_{sep} \log\left(\frac{p_{sep}}{114.7}\right)\right]. \tag{3.5}$$

The oil FVF is estimated on the following correlations that come from Vazquez and Beggs (1980) study as well

$$B_o = B_{ob} exp\left[c_o (p_{bp} - p_i\right], \tag{3.6}$$

where B_{ob} – oil FVF at bubble point pressure and could be calculated as

$$B_{ob} = 1 + D_1 R_s + D_2 (T - 60)\left(\frac{\gamma_o}{\gamma_{gs}}\right) + D_3 R_s (T - 60)\left(\frac{\gamma_o}{\gamma_{gs}}\right), \tag{3.7}$$

and c_o – oil isothermal compressibility that can be estimated as

$$c_o = \frac{-1433 + 5R_s + 17.2T - 1180\gamma_{gs} + 12.61\gamma_o}{10^5 p}. \tag{3.8}$$

The coefficients *C*, *A*, and *D* in questions (3.3), (3.4), and (3.7) are listed in Table 3.4 and depends on oil API gravity.

Table 3.3. Initial reservoir and bubble point pressure input.

Initial reservoir pressure and bubble point pressure	**Symbol**
Reservoir depth, ft	H
Initial reservoir pressure*, psia	p_i
Reservoir temperature*, F	T
Vazquez & Beggs correlations:	
Separator pressure, psia	p_{sep}
Separator temperature, F	T_{sep}
Gas specific gravity (p_{sep}, T_{sep})	γ_{gp}
Oil API gravity	API
Solution GOR*, scf/STB	R_s
Bubble point pressure*, psi	p_{bp}
Oil FVF*, bbl/STB	B_o
Water FVF, bbl/STB	B_w

*parameter can be estimated from required input values

Table 3.4. Vazques and Beggs correlation coefficients

Vazques and Beggs coefficient	**Value**	
	$\gamma_{oAPI} \leq 30$	$\gamma_{oAPI} > 30$
C_1	0.0362	0.0178
C_2	1.0937	1.187
C_3	25.724	23.931
A_1	27.64	56.06
A_2	1.0937	1.187
A_3	11.172	10.393
D_1	4.667×10^{-4}	4.67×10^{-4}
D_2	1.751×10^{-5}	1.1×10^{-5}
D_3	-1.811×10^{-8}	1.337×10^{-9}

If the value of the minimal principal horizontal stress in not known, the formation is assumed to be under uniaxial strain conditions and the minimum horizontal stress is estimated based on the equations (2.5) and (2.6). The required input for minimum horizontal stress estimation is shown in Table 3.5.

Table 3.5. Minimum horizontal stress parameters

Minimum horizontal stress	**Symbol**
Rock density, lb/ft3	ρ
Poisson Ration	υ
Absolute minimum horizontal stress*, psi	σ_{hmin}

*parameter can be estimated from required input values

The waterflood performance calculations are constrained by the maximum pressure drop between injector and producer. Taking into account the assumptions listed in the beginning of this section the maximum pressure drop can be found as

$$\Delta p_{I-P} = \sigma_{hmin} - p_{bp} - p_{injs}, \tag{3.9}$$

where p_{injs} – injection pressure safety factor to prevent injection pressure reaching the value of minimum horizontal stress. The required input and calculated parameters are shown in Table 3.6.

Table 3.6. Waterflood pressure constraint

Waterflood constraints	**Symbol**
Injection pressure safety factor, psi	p_{injs}
Maximum injection pressure*, psi	p_{inj}
Maximum I-P pressure drop*, psi	$\Delta p_{I\text{-}P}$

*parameter can be estimated from required input values

The waterflood performance calculations are done on the basis of the reservoir volume between one producing and one injecting fracture planes, requiring the dimension parameters shown in Table 3.7. We assume that fracture height (h_f) is equal or less than the reservoir thickness.

Table 3.7. Plane to plane dimension parameters

Reservoir unit dimensions	**Symbol**
Distance between I-P fractures, ft	$x_{s(I-P)}$
Fracture height, ft	h_f
½ Fracture length, ft	x_f

The economic analysis requires the input of the length of the well's horizontal section (L_w). We assume that in a single pattern configuration all three wells have the same length. We calculate the required amount of proppant based on the dimensionless infinite fracture conductivity index

$$C_{fD} = \frac{k_f w}{k x_f}, \tag{3.10}$$

where w – fracture width. Table 3.8 indicates the required fracture and proppant properties.

Table 3.8. Fracture and proppant properties

Fracture and proppant properties	**Symbol**
Dimensionless infinite fracture conductivity	C_{fD}
Specific gravity of proppant material	ρ_{prop}
Porosity of proppant pack, fraction	$\emptyset_f$
Proppant pack permeability, md	k_f
Max proppant diameter, inch	D_{pmax}

Finally, economic parameters associated with drilling, completion, and stimulation costs are required to calculate the investments per well pattern. As well, the market price of the crude oil and annual discount rate are required to estimate profit. Table 3.9 shows required economic input parameters.

Table 3.9. Economic parameters

Economic Parameters	**Symbol**
Vertical well construction cost, $/ft	C_{wv}
Horizontal well construction cost, $/ft	C_{wh}
Pumping charges, $/frac	C_{pump}
Proppant cost, $/lbm	C_{prop}
Annual discount rate, fraction	r
Oil market price, $/STB	P

Based on Table 3.9 input and estimated production profile the net present value cash flow is calculated as

$$NPV(i,N) = \sum_{t=o}^{N} \frac{R_t}{(1+i)^t}, \tag{3.11}$$

where R_t is net cash flow, i is the discount rate, and N is the total number of periods.

The model outputs include production rate over time per reservoir unit and per pattern (for pressure controlled waterflood wells) or pressure drop (for controlled injection rate), water breakthrough time, recovery factor and water cut versus time or versus pore volume injected. Appendix A shows the input screen of the screening tool, Appendix B provides equations and correlations for default values computed from required inputs, and Appendix B provides equations for calculating waterflood performance at constant pressure drop.

Linear waterflood at constant pressure drop leads to the maximum rate possible, thus the most economical way to implement waterflooding. At the same time, this approach

is easy to implement from the operational point of view and that's why it is most popular at the field.

The analytical screening tool model for constant injection rate has the same input set of parameters and requirements and estimates the same reservoir or fluid parameters as was described above. However, in contrast to the constant pressure drop solution when rate varies with time, the constant rate solution varies the applied pressure drop in order to keep the rate constant.

With production and injection rate held constant, the pressure drop across the system increases linearly until the water breakthrough. The pressure drop reaches the maximum value at the water breakthrough and then starts decreasing. Our model is constrained by the maximum injection pressure at the injector and the minimum bottom hole pressure at the producer. So, we have to find iteratively the constant injection (and production) rate at which the maximum pressure drop across the system would be within the constraints of our system. The pressure behavior across the system of waterflood at the constant injection rate and constant pressure drop is shown in Figure 3.7. Appendix D provides equations for calculating waterflood performance at the constant injection rate.

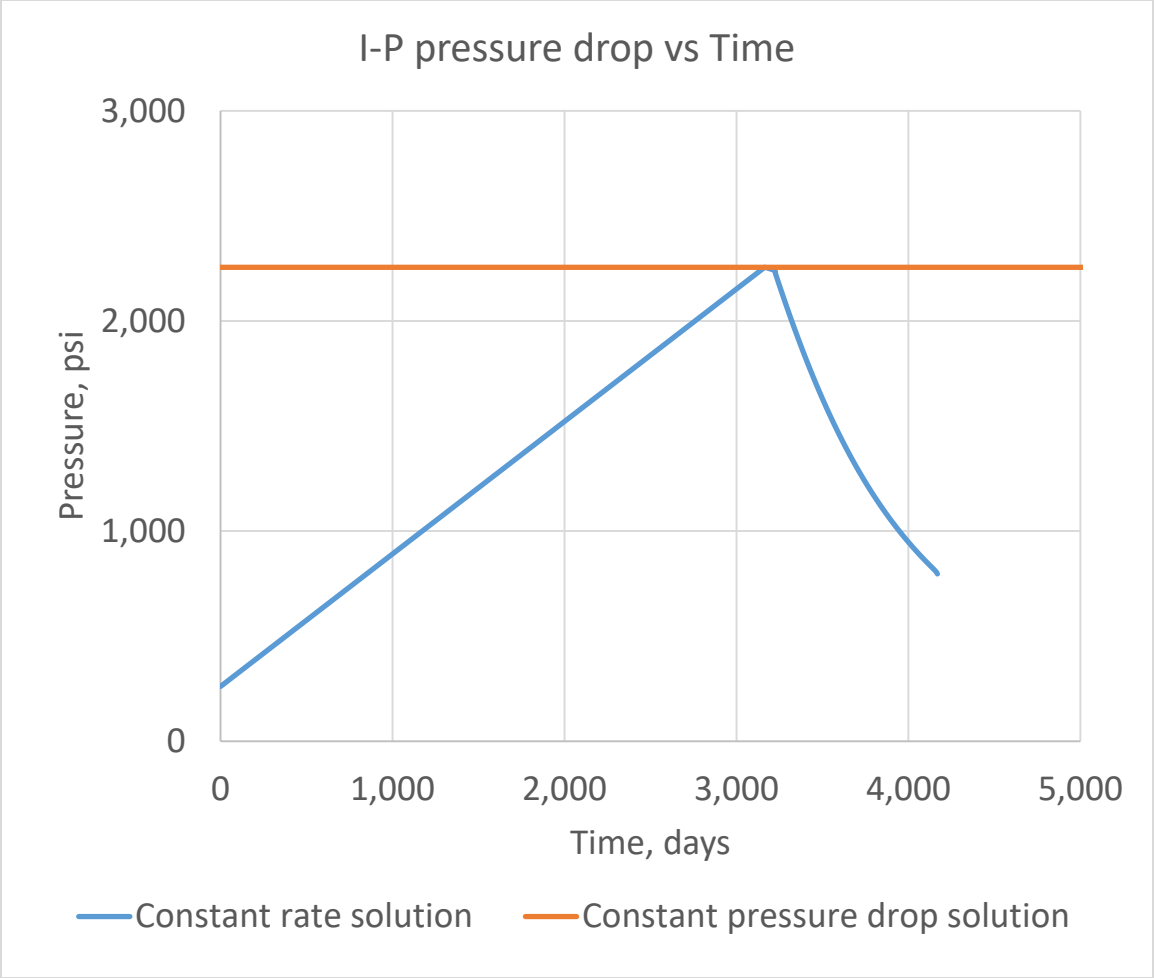

Figure 3.7. Comparison of pressure trends for linear waterflood.

As could be inferred from Figure 3.7 the waterflood at the constant pressure drop will significantly outperform the waterflood at constant rate with all other variable being the same. Figure 3.8 shows the same result.

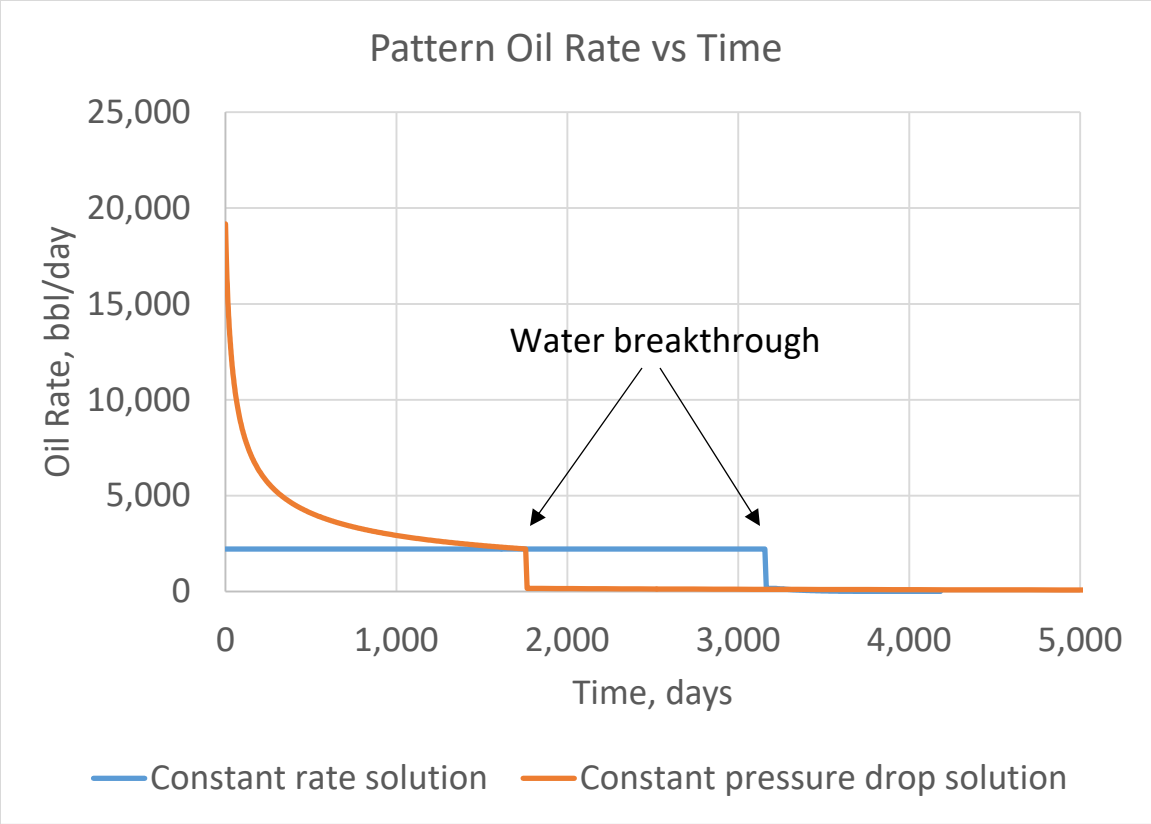

Figure 3.8. Comparison of oil production rate for linear waterflood.

3.4 Chapter summary

This chapter reviewed the commonly known MTFHW pattern types and their application for secondary recovery. A new pattern expected to provide superior performance during waterflooding was introduced. An analytical screening model to assess proposed well pattern performance and economics at constant pressure drop and constant injection rate was described. The advantage of waterflooding technique at constant pressure drop was explained, and for that reason, the waterflood at constant pressure drop will be used in the following chapter to assess the new pattern performance and its applicability to the major US shale plays.

CHAPTER 4 WELL PATTERN APPLICATION AND SENSITIVITY

In this chapter, the developed analytical screening tool will be used to determine performance and economics of the designed well pattern for different pattern geometries and reservoir conditions, as well as to check the pattern applicability for major US shale plays based on the publically available rock and fluid properties.

4.1 Sensitivity to reservoir permeability

Before running the sensitivity cases, we need to set up the artificial data set for the base case. The particular data in the base data set is not of great importance because the main goal of this section is to look at the behavior trends rather than particular numbers.

However, it worth explaining the choice of several parameters. The base case permeability is set to 0.1 md. The permeability equal or below that value is in the range of the tight (unconventional) reservoirs and the permeability greater than 0.1 md is in the range of conventional reservoirs. Reservoir porosity is assumed to be 12% which is acceptable for both conventional and unconventional reservoirs. The distance between injecting and producing fractures is assumed to be 50 ft, thus the fracture spacing per well is 100 ft. The length of the horizontal section of the well is set to be 5,280 ft and the reservoir depth is set to 10,000 ft. Input parameters that could be estimated with correlations were not manually changed. Appendix B shows the correlations and equations used to develop default inputs. All the values of the input parameters for the base case are listed in Table 4.1.

Table 4.1. Base case input parameters.

Parameter	Symbol	Value
Rock and Fluid Properties		
Porosity, fraction	ϕ	0.12
Permeability, md	k	0.1
Oil viscosity, cp	μ_o	0.42
Water viscosity, cp	μ_w	0.57
Water salinity, wt. %	S	6
Relative Permeability (Corey)		
Water Corey exponent	n_w	4
Oil Corey exponent	n_o	4
Connate water saturation, fraction	S_{wc}	0.25
Residual oil saturation, fraction	S_{or}	0.2
Water relative permeability at residual oil saturation	$k_{rw}(S_{or})$	0.45
Oil relative permeability at connate water saturation	$k_{ro}(S_{wc})$	1
Initial Reservoir Pressure and Bubble Point Pressure		
Reservoir depth (mid oil column), ft	H	10,000
Initial reservoir pressure, psia	p_i	4,515
Reservoir temperature, F	T	160
Vazquez & Beggs correlations		
Separator pressure, psia	p_{sep}	400
Separator temperature, F	T_{sep}	100
Gas specific gravity (p_{sep}, T_{sep})	γ_{gp}	0.78
Oil API gravity	API	35
Solution GOR, scf/STB	R_s	1,284
Bubble point pressure, psi	p_{bp}	4,463
Oil FVF, bbl/STB	B_o	1.6
Water FVF, bbl/STB	B_w	1
Minimum Horizontal Stress		
Rock density, lb/ft3	ρ	165
Poisson Ration	υ	0.3
Absolute minimum horizontal stress, psi	σ_{hmin}	6,768
Waterflood Constraints		
Injection pressure safety factor, psi	p_{injs}	50
Maximum injection pressure, psi	p_{inj}	6,718
Maximum I-P pressure drop, psi	$\Delta_{pI\text{-}P}$	2,256

Table 4.1 (continued).

Reservoir Unit Dimensions		
Distance between I-P fractures, ft	$x_{s(I-P)}$	50
Fracture height, ft	h_f	250
½ Fracture length, ft	x_f	150
Pattern Geometry		
Horizontal well length, ft	L_w	5,280
Fracture properties		
Dimensionless infinite fracture conductivity	C_{fD}	50
Specific gravity of proppant material	ρ_{prop}	2.65
Porosity of proppant pack, fraction	ϕ_f	0.38
Proppant pack permeability, md	k_f	150,000
Max proppant diameter, inch	D_{pmax}	0.031
Economic parameters		
Vertical well construction cost, $/ft	C_{wv}	250
Horizontal well construction cost, $/ft	C_{wh}	500
Pumping charges, $/frac	C_{pump}	30,000
Proppant cost (20/40 ceramic, 150 Darcy), $/lbm	C_{prop}	1.5
Annual discount rate, fraction	r	0.1
Oil market price, $/STB	P	50

For the given base data set, the estimated recovery factor is about 56% at the time of the water breakthrough. Due to piston like displacement, the water cut jumps above 90% after water breakthrough occurs (Figure 3.9).

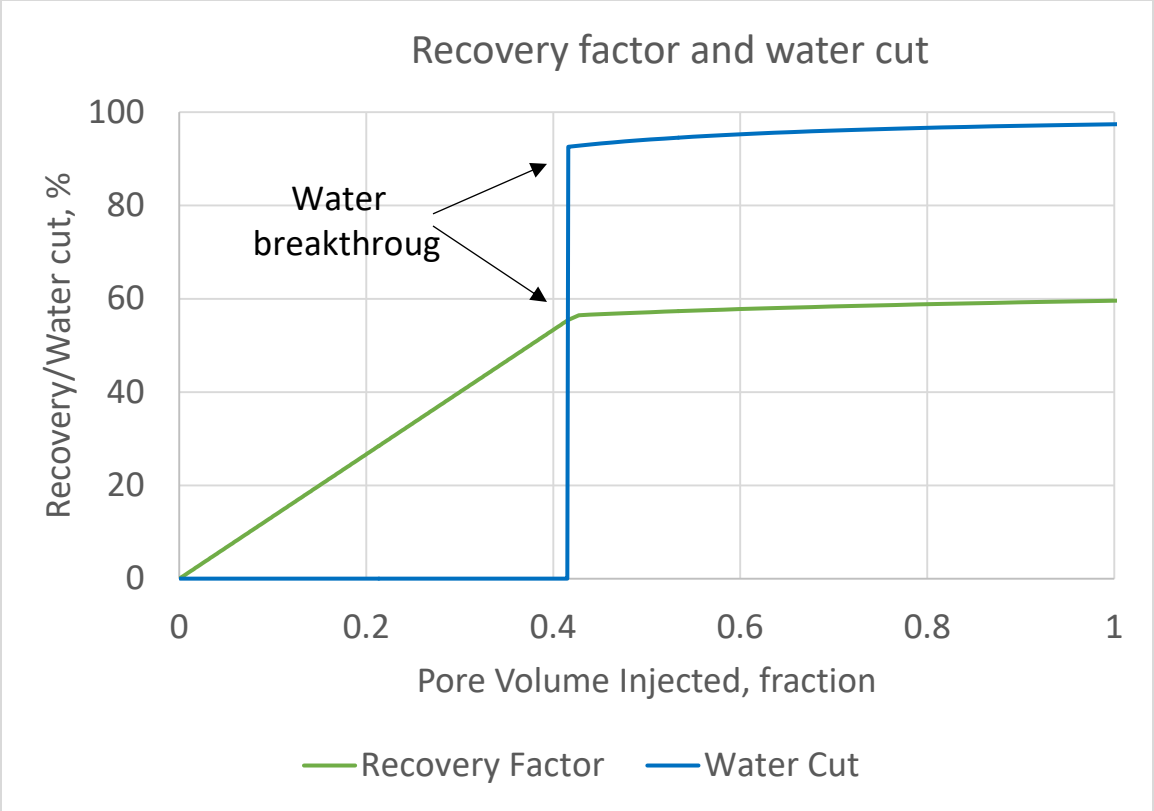

Figure 4.1. Base case recovery factor and water cut.

Table 4.2 shows sensitivity of the base case to the input permeability value. The reservoir permeability was varied both above and below the base case value until the resultant production was unrealistic or economics was negative.

Table 4.2. Well pattern sensitivity to the reservoir permeability.

Performance indicator	**Reservoir permeability, md**				
	0.0001	**0.001**	**0.01**	**0.1**	**1**
Water breakthrough time, days	176,467	17,646	1,764	176	17
Initial (max) oil production rate per reservoir unit, bbl/d	0.456	4.6	46	456	4,564
Initial (max) oil production rate per pattern, bbl/d	192	1,913	18,779	160,901	841,185
NPV @ BT or NPV @ 3 years, MM$	-34	-6	105	165	-16

The results in Table 4.2 show the water breakthrough time and the initial oil rate linearly depend on the value of reservoir permeability. Figure 4.1 shows the dynamics of the pattern oil rate for the first 10 years.

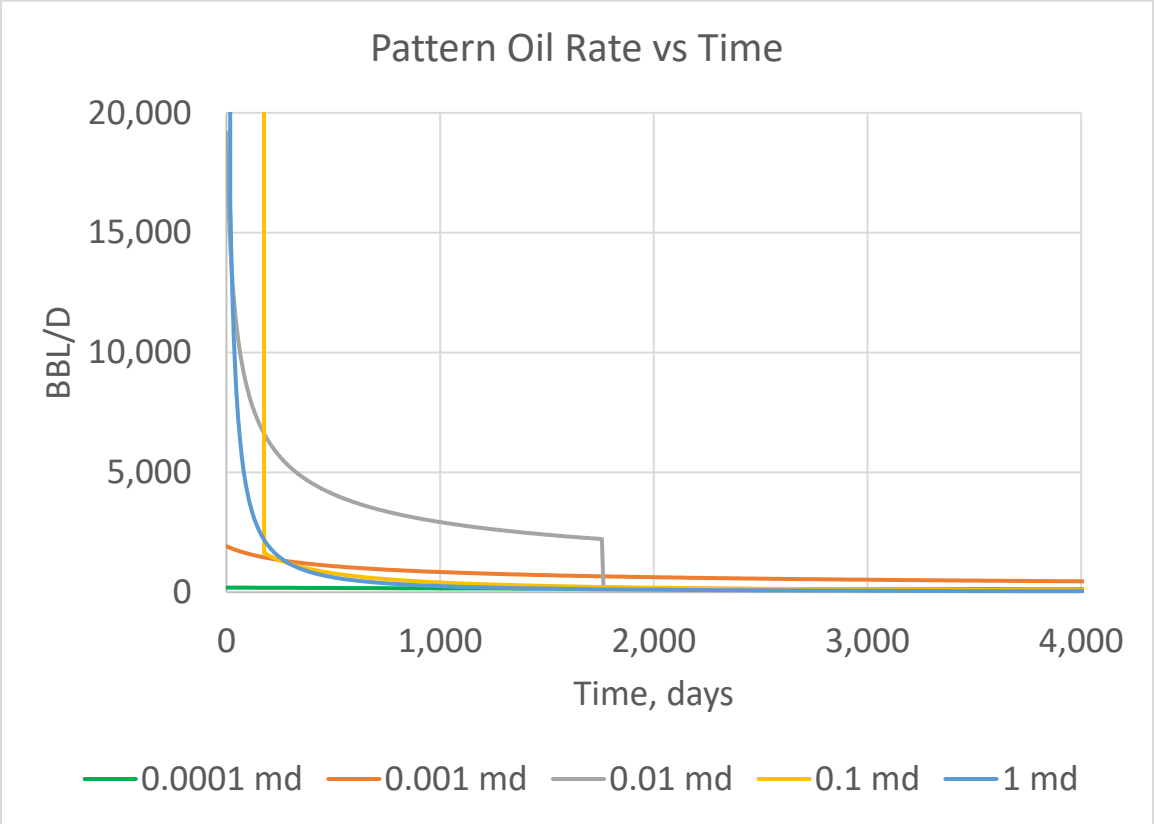

Figure 4.2. Well pattern oil rate for different reservoir permeability.

The NPV value depends on the speed of oil recovery and the value of initial investments. In the given cases with different reservoir permeability, the initial investments vary with the amount of proppant required to create fractures with infinite conductivity.

Considering the results of the given base case, the realistic application of the designed pattern is in the reservoirs with permeability of 0.01 md. This conclusion is only applicable

to the particular data set. The change in PVT or reservoir properties, the geometry of the pattern or economic assumptions can significantly extend or contract the applicability of the designed pattern.

4.2 Sensitivity to different pattern geometries

In the previous section, we looked at the pattern sensitivity to the reservoir permeability. Normally, permeability is not one of the parameters that the engineer can adjust. In this section, we will run sensitivities on the parameters that can be designed before the pattern is implemented in the field, such as well spacing and fracture spacing.

4.2.1 Well spacing sensitivity

In these sensitivity runs the same data set specified in Table 4.1 will be used with only one change – reservoir permeability is set to 0.01 md. The fracture half length (x_f) will be varied representing the distance between the wells. Four cases with different well spacing were set up: 100 ft, 150 ft, 300 ft, and 600 ft. The result of the sensitivity runs is shown in Table 4.3 and Figure 4.3.

Table 4.3. Well pattern sensitivity to the well spacing.

Performance indicator	**Well spacing, ft**			
	100	**150**	**300**	**600**
Water breakthrough time, days	1,764	1,764	1,764	1,764
Initial (max) oil production rate per reservoir unit, bbl/d	30	46	91	183
Initial (max) oil production rate per pattern, bbl/d	12,519	18,779	37,558	75,117
NPV @ BT or NPV @ 3 years, MM$	64	105	231	482
NPV @ BT or NPV @ 3 years, MM$ (4 x proppant cost)	25	48	116	253

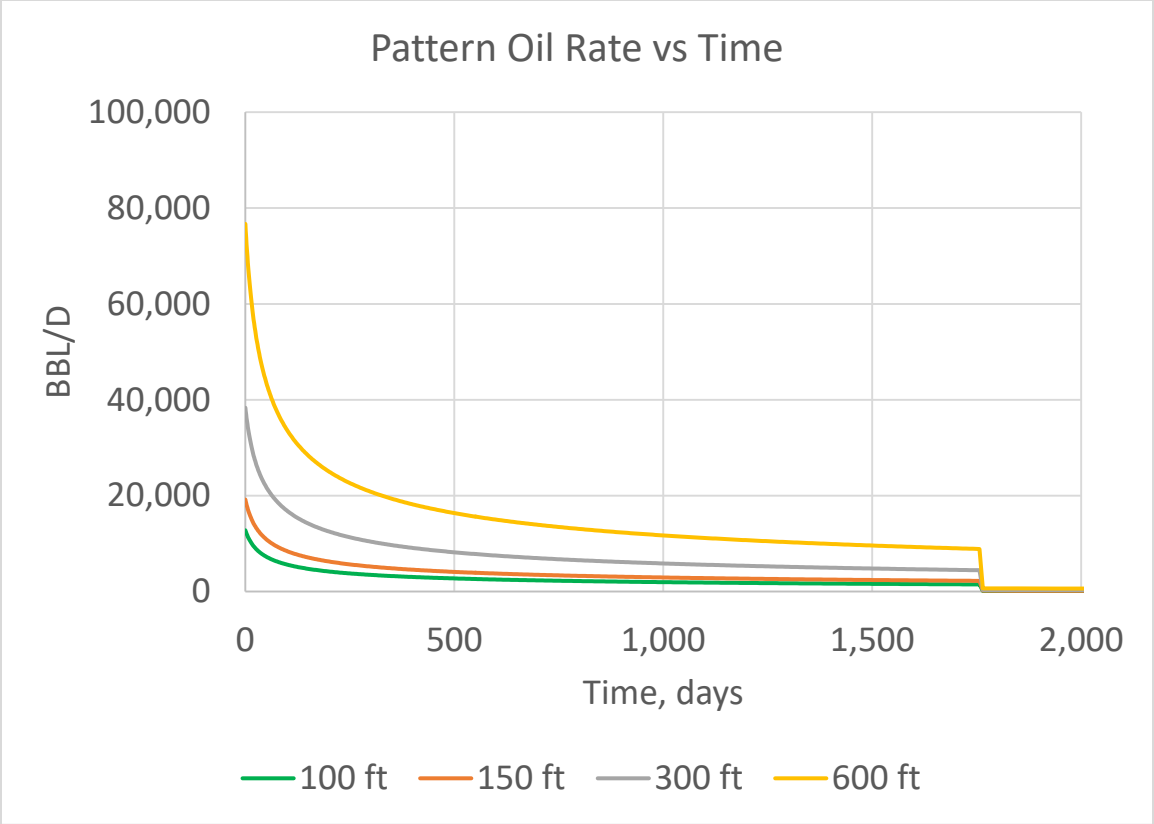

Figure 4.3. Well pattern oil rate for different well spacing.

The analysis of Table 4.3 and Figure 4.3 shows that with the increase of well spacing the flow area of the each water flooded reservoir unit is increasing and the oil rate increases proportionally to the increase of well spacing. The breakthrough timing is unaffected by the change in well spacing. That means that the main limiting factor for the wider well spacing is the operational limits in creating water-injecting fractures, as they are twice the length of the producing fractures. The proppant cost is another important parameter in estimating NPV of the project. The cost of proppant was increased 4 times from 1.5 to 6 $/lb. This change in cost significantly decreased NPV of the projects but the ranking of the projects stays the same with the case of 600 ft well spacing being the most profitable.

4.2.2 Fractures spacing sensitivity

In these sensitivity runs the same data set specified in Table 4.1 will be used with only one change – reservoir permeability is set to 0.01 md. The distance between injecting and producing fractures ($x_{s(I-P)}$) will be varied. Four cases with different I-P fracture spacing were set up: 25 ft, 50 ft, 100 ft, and 200 ft. The result of the sensitivity runs is shown in Table 4.4 and Figure 4.4.

Table 4.4. Well pattern sensitivity to the I-P fracture spacing.

Performance indicator	I-P fracture spacing, ft			
	25	50	100	200
Water breakthrough time, days	441	1,764	7,058	28,234
Initial (max) oil production rate per reservoir unit, bbl/d	91	46	23	11
Initial (max) oil production rate per pattern, bbl/d	71,294	18,779	4,722	1,185
NPV @ BT or NPV @ 3 years, MM$	140	105	34	1.8
NPV @ BT or NPV @ 3 years, MM$ (4 x proppant cost)	25	48	5	-13

The analysis of Table 4.4 and Figure 4.4 shows that with the increase of fracture spacing the oil rate decreases proportionally on the basis of the one reservoir unit, but varies on the well pattern level as each pattern configuration has a different number of reservoir units. The breakthrough timing is increasing following the power low with the increase of the fracture spacing. Due to a significant decrease in the oil rate, the economics of the cases with wider fracture spacing declining rapidly. It could be concluded that the tighter fracture spacing positively affecting production oil rate and economics of the project in relatively tight oil reservoirs. The increased cost of proppant significantly affects the profitability of the project, but the ranking of the projects stays the same with the case of 25 ft I-P fracture spacing being the most profitable. However, in the reservoir with

permeability in conventional ranges, the flow rate for the case with small fracture spacing could be unrealistically high (0.1 md and 1 md cases in Table 4.2) or the investments in creating fractures with infinite conductivity could overweigh the benefits.

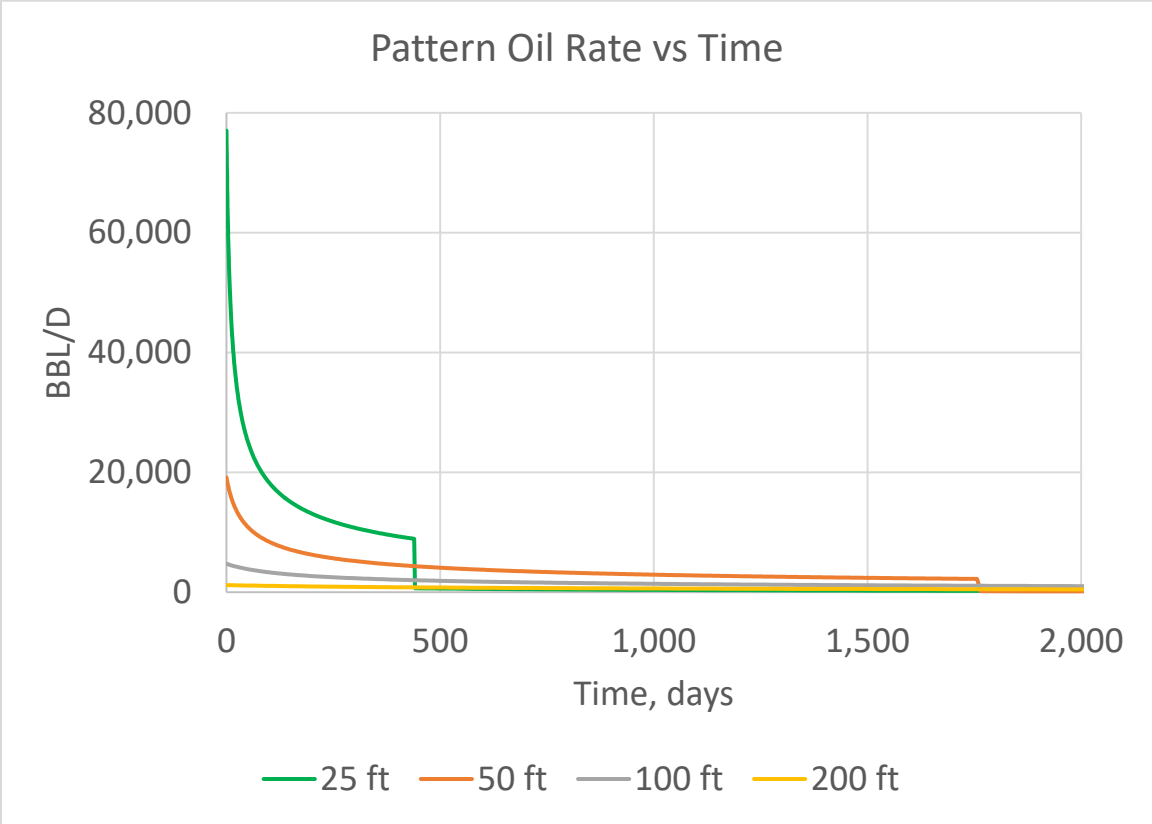

Figure 4.4. Well pattern oil rate for different I-P fracture spacing.

4.2 Well pattern application to the major US shale plays

In this section, the publically available data about the major US shale development areas will be used to do sensitivity runs on the proposed well pattern design with different geometries. As we learned in section 4.2.1 the increasing well spacing is generally has a positive effect on the waterflood performance in formations with low permeability. Cipolla, Lolon, and Mayerhofer (2009) noted that fracture length in tight formations could

reach 1500 ft and even longer. However, we will constrain the geometry of designed patterns to the 2 simple cases. The first one will have, commonly drilled nowadays, wells with the horizontal section of 1 mile long and well spacing of 165 ft and the second one will have the wells with the same length of the horizontal section and the well spacing of 330 ft. In the first case, the production area is 40 ac per production well and in the second case is 80 ac. The I-P fracture spacing will be equal to 50 ft and 100 ft for both cases. These sensitivity runs will allow us to assess the effect of well spacing and fracture spacing on the performance of the pattern.

4.2.1 Eagle Ford shale

The Eagle Ford shale formation in South Texas runs from the US-Mexico border north of Laredo in a narrow band extending northeast for several hundred miles to just north of Houston as shown in Figure 4.5. It is located directly below the Austin Chalk. The thickness of the Eagle Ford shale could reach 500 ft with the average of about 250 feet. The more active part of the region is mainly in McMullen, Maverick, Dimmit, La Salle, Karnes, Live Oak, and Atascosa counties. The formation produces both natural gas and oil (OGJ 2016c).

The number of studies such as Yang et al. (2014), Morsy, Sheng and Soliman (2013), Mullen, Lowry and Nwabuoku (2010), Whitson and Sunjerga (2012), Honarpour et al. (2012), Gong et al. (2013), and Braun et al. (2014) were published with descriptions of liquid reach shales and Eagle Ford in particular. The data from these studies is a basis for the input parameters in analytical screening tool and it is summarized in Table 4.5.

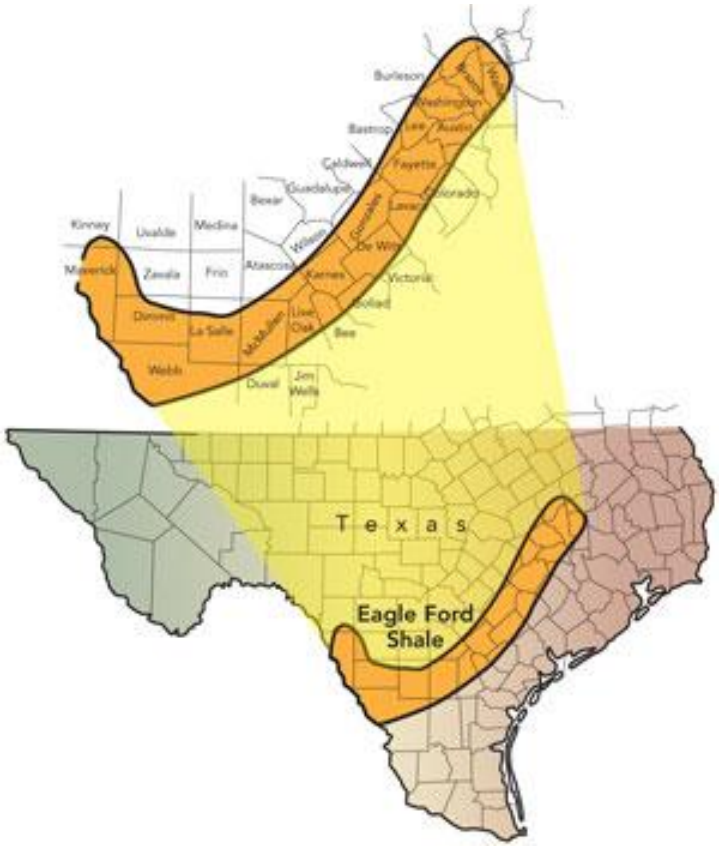

Figure 4.5. Eagle Ford shale location map

Table 4.5. Eagle Ford shale input parameters.

Parameter	Symbol	Value
Rock and Fluid Properties		
Porosity, fraction	ϕ	0.085
Permeability, md	k	0.0008
Oil viscosity, cp	μ_o	0.3
Water viscosity, cp	μ_w	0.38
Water salinity, wt. %	S	6
Relative Permeability (Corey)		
Water Corey exponent	n_w	4
Oil Corey exponent	n_o	4
Connate water saturation, fraction	S_{wc}	0.25
Residual oil saturation, fraction	S_{or}	0.25
Water relative permeability at residual oil saturation	$k_{rw}(S_{or})$	0.45
Oil relative permeability at connate water saturation	$k_{ro}(S_{wc})$	1

Table 4.5 (continued).

Initial Reservoir Pressure and Bubble Point Pressure		
Reservoir depth (mid oil column), ft	H	10,000
Initial reservoir pressure, psia	p_i	5,000
Reservoir temperature, F	T	244
Vazquez & Beggs correlations		
Separator pressure, psia	p_{sep}	400
Separator temperature, F	T_{sep}	100
Gas specific gravity (p_{sep}, T_{sep})	γ_{gp}	0.78
Oil API gravity	API	42.1
Solution GOR, scf/STB	R_s	1,007
Bubble point pressure, psi	p_{bp}	3,342
Oil FVF, bbl/STB	B_o	1.52
Water FVF, bbl/STB	B_w	1
Minimum Horizontal Stress		
Rock density, lb/ft3	ρ	165
Poisson Ration	υ	0.3
Absolute minimum horizontal stress, psi	σ_{hmin}	6,968
Waterflood Constraints		
Injection pressure safety factor, psi	p_{injs}	50
Maximum injection pressure, psi	p_{inj}	6,918
Maximum I-P pressure drop, psi	$\Delta_{pI\text{-}P}$	3,575
Fracture properties		
Dimensionless infinite fracture conductivity	C_{fD}	50
Specific gravity of proppant material	ρ_{prop}	2.65
Porosity of proppant pack, fraction	ϕ_f	0.38
Proppant pack permeability, md	k_f	150,000
Max proppant diameter, inch	D_{pmax}	0.031
Economic parameters		
Vertical well construction cost, $/ft	C_{wv}	250
Horizontal well construction cost, $/ft	C_{wh}	500
Pumping charges, $/frac	C_{pump}	30,000
Proppant cost (20/40 ceramic, 150 Darcy), $/lbm	C_{prop}	1.5
Annual discount rate, fraction	r	0.1
Oil market price, $/STB	P	50

The summary of compared pattern geometries is shown in Table 4.6.

Table 4.6. Eagle Ford assessed pattern geometries.

Dimensions	Cases (A_w: $x_{s(I-P)}$)			
	40 ac: 50 ft	40 ac: 100 ft	80 ac: 50 ft	80 ac: 100 ft
Distance between I-P fractures, ft	50	100	50	100
Fracture height, ft	250	250	250	250
½ Fracture length, ft	165	165	330	330
Horizontal well length, ft	5,280	5,280	5,280	5,280

The oil rate and net present value estimations for Eagle Ford input parameters and different pattern geometries are shown in Figure 4.6 and 4.7.

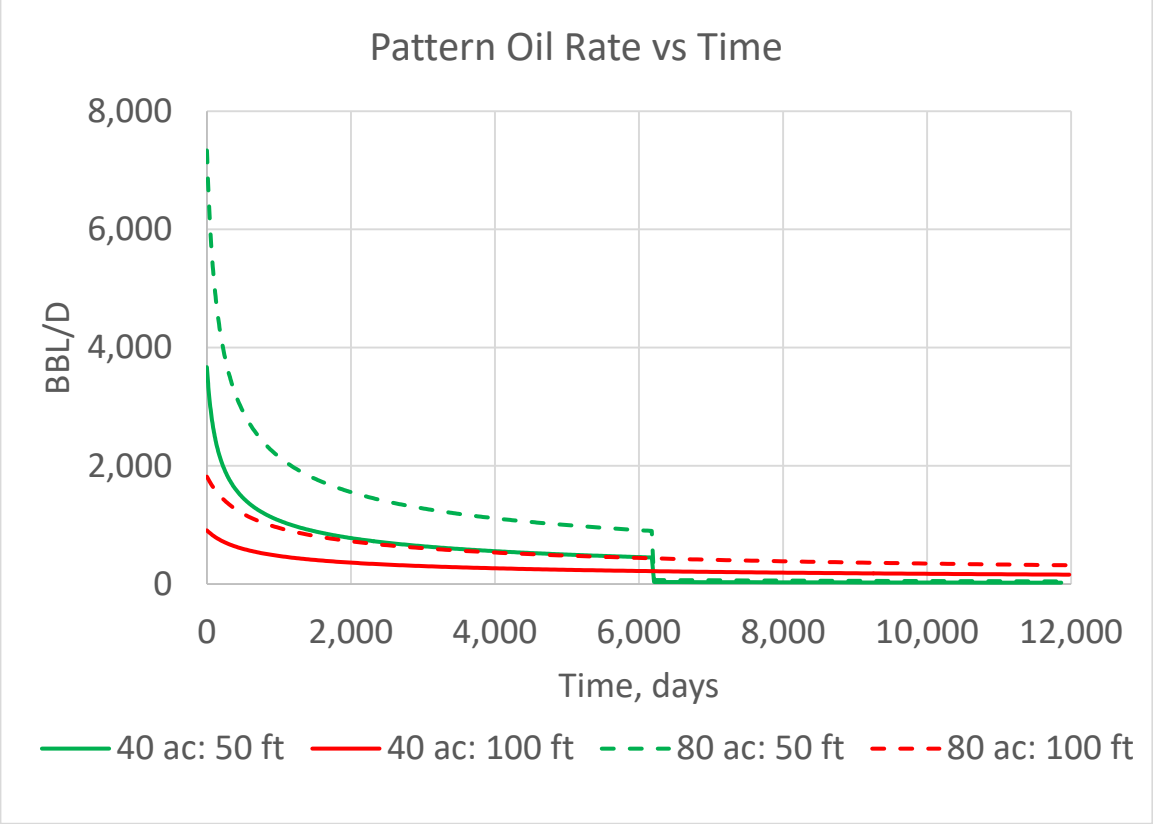

Figure 4.6. Eagle Ford shale production oil rate estimation.

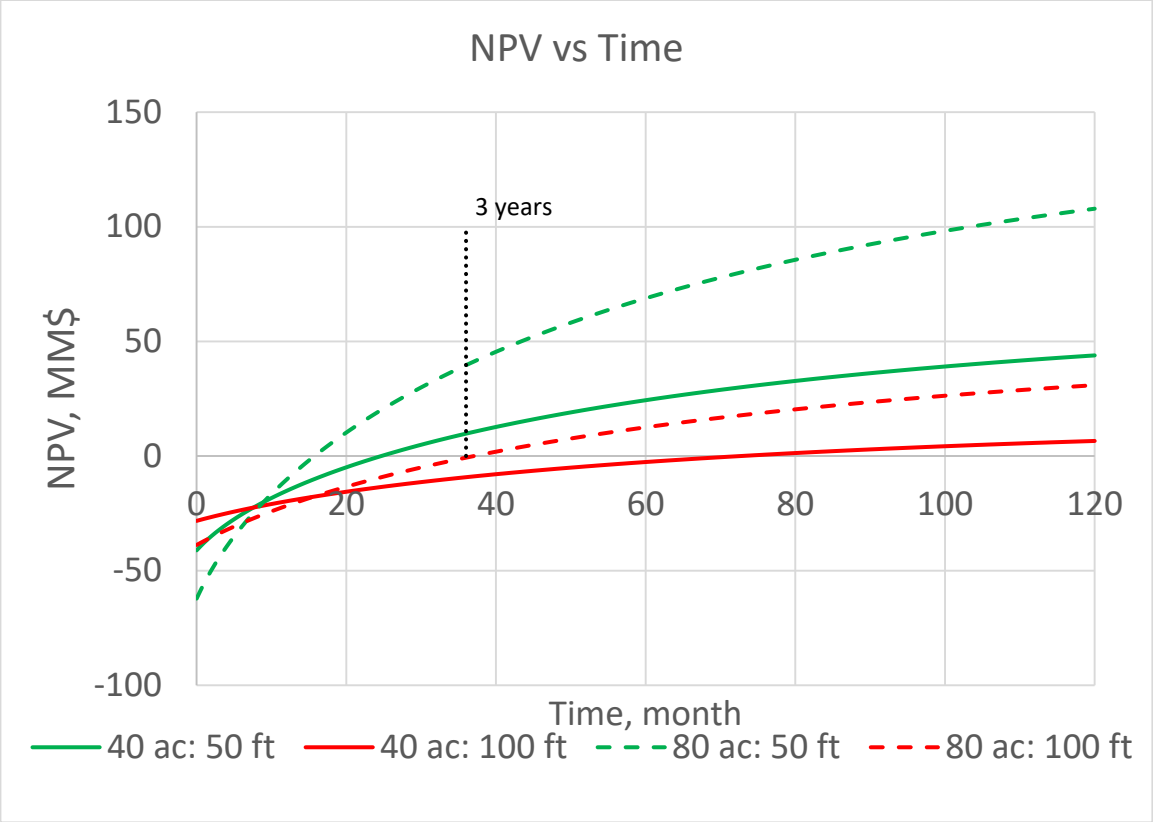

Figure 4.7. Eagle Ford shale NPV estimation.

The analysis of the results presented in Figure 4.6 and 4.7 shows that increased I-P fracture spacing negatively affecting production rate and, as a result, the economics of the well pattern. As expected, the increase in well spacing improves oil flowrate and, as a result, economics. However, the more important conclusion that can be drawn from the results is that the designed pattern is a viable option for enhanced oil recovery in Eagle Ford shale formation and can be economical at I-P fracture spacing of 50 ft.

4.2.2 Barnett shale

The Barnett shale in north-central Texas lies in the Fort Worth Basin (see Figure 4.8). Discovered in the 1950s, the Barnett was not commercially viable until the 1980s. Some geologists believe the formation could hold 30 trillion cubic feet of natural gas. A significant part of the drilling has occurred in the Fort Worth metro area (OGJ 2016b).

Drilling in the Barnett shale intensified in the past decade as modern horizontal drilling and hydraulic fracturing techniques were perfected for drilling in shale. Two years ago, 70% of all US gas shale production came from the Barnett, but that percentage of the total has been declining as production has risen in other plays. The Barnett shale is mainly associated with success in gas production; however, there are some relatively small accumulations of oil and some attempts to produce them have been made. The oil window in the Barnett shale is relatively small – less than 200 ft thick and with matrix permeability measured in nanodarcies.

The summary of estimated Barnett shale properties is given in Table 4.7 and based on the number of research publication such as Kale, Rai and Sondergeld (2010), Cipolla, Lolon and Erdle (2010), Nieto, Bercha and Chan (2009), Frantz et al. (2005) and Montgomery et al. (2005).

Figure 4.8. Barnett shale location map.

Table 4.7. Barnett shale input parameters.

Parameter	Symbol	Value
Rock and Fluid Properties		
Porosity, fraction	ϕ	0.06
Permeability, md	k	0.00005
Oil viscosity, cp	μ_o	0.35
Water viscosity, cp	μ_w	0.59
Water salinity, wt. %	S	6
Relative Permeability (Corey)		
Water Corey exponent	n_w	4
Oil Corey exponent	n_o	4
Connate water saturation, fraction	S_{wc}	0.25
Residual oil saturation, fraction	S_{or}	0.25
Water relative permeability at residual oil saturation	$k_{rw}(S_{or})$	0.45
Oil relative permeability at connate water saturation	$kro(Swc)$	1

Table 4.7 (continued).

Initial Reservoir Pressure and Bubble Point Pressure		
Reservoir depth (mid oil column), ft	H	7,000
Initial reservoir pressure, psia	p_i	4,000
Reservoir temperature, F	T	150
Vazquez & Beggs correlations		
Separator pressure, psia	p_{sep}	400
Separator temperature, F	T_{sep}	100
Gas specific gravity (p_{sep}, T_{sep})	γ_{gp}	0.78
Oil API gravity	API	40
Solution GOR, scf/STB	R_s	1,400
Bubble point pressure, psi	p_{bp}	3,947
Oil FVF, bbl/STB	B_o	1.69
Water FVF, bbl/STB	B_w	1
Minimum Horizontal Stress		
Rock density, lb/ft3	ρ	165
Poisson Ration	υ	0.3
Absolute minimum horizontal stress, psi	σ_{hmin}	5,083
Waterflood Constraints		
Injection pressure safety factor, psi	p_{injs}	50
Maximum injection pressure, psi	p_{inj}	5,033
Maximum I-P pressure drop, psi	$\Delta_{pI\text{-}P}$	1,086
Fracture properties		
Dimensionless infinite fracture conductivity	C_{fD}	50
Specific gravity of proppant material	ρ_{prop}	2.65
Porosity of proppant pack, fraction	ϕ_f	0.38
Proppant pack permeability, md	k_f	150,000
Max proppant diameter, inch	D_{pmax}	0.031
Economic parameters		
Vertical well construction cost, $/ft	C_{wv}	250
Horizontal well construction cost, $/ft	C_{wh}	500
Pumping charges, $/frac	C_{pump}	30,000
Proppant cost (20/40 ceramic, 150 Darcy), $/lbm	C_{prop}	1.5
Annual discount rate, fraction	r	0.1
Oil market price, $/STB	P	50

The summary of compared pattern geometries is shown in Table 4.8.

Table 4.8. Barnett assessed pattern geometries.

Dimensions	Cases (A_w: $x_{s(I-P)}$)			
	40 ac: 50 ft	40 ac: 100 ft	80 ac: 50 ft	80 ac: 100 ft
Distance between I-P fractures, ft	50	100	50	100
Fracture height, ft	200	200	200	200
½ Fracture length, ft	165	165	330	330
Horizontal well length, ft	5,280	5,280	5,280	5,280

The oil rate and net present value estimations for Barnett input parameters and different pattern geometries are shown in Figure 4.9 and 4.10.

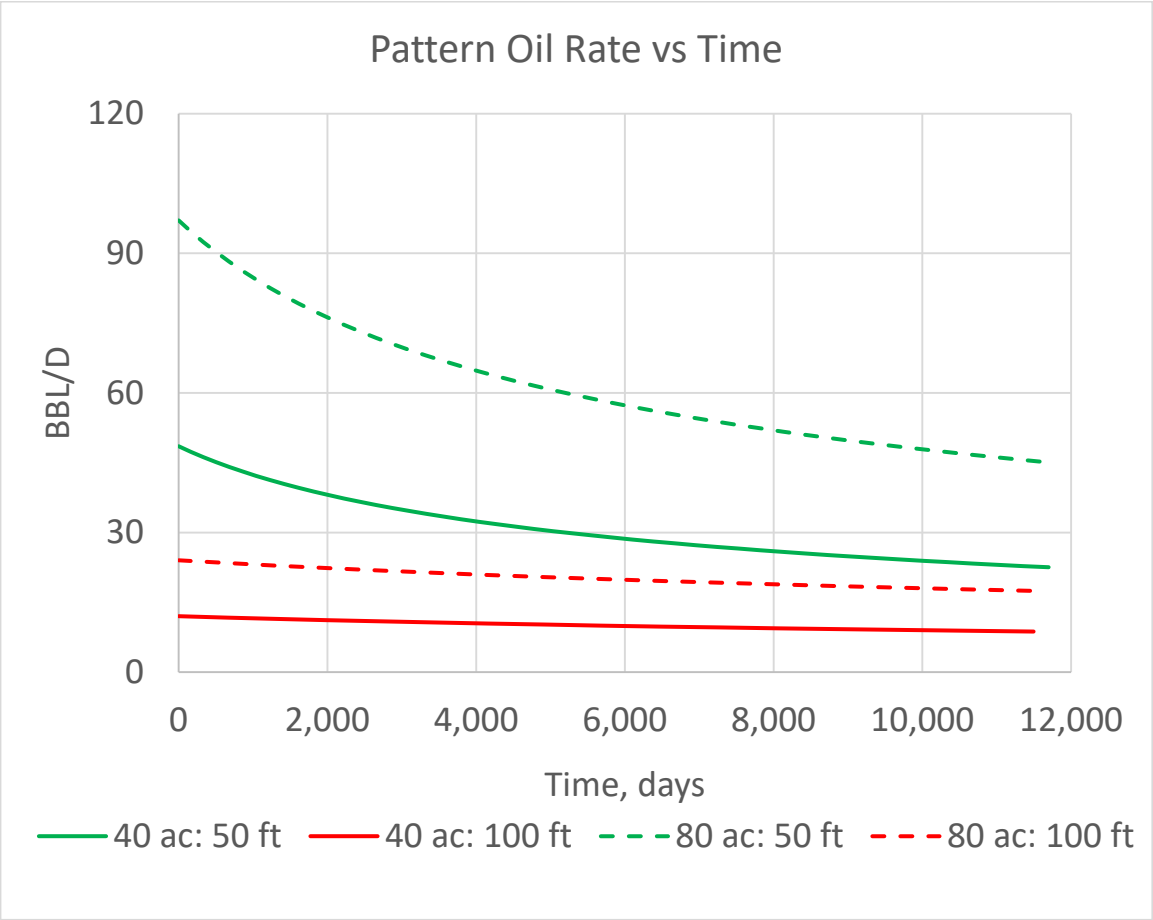

Figure 4.9. Barnett shale production oil rate estimation.

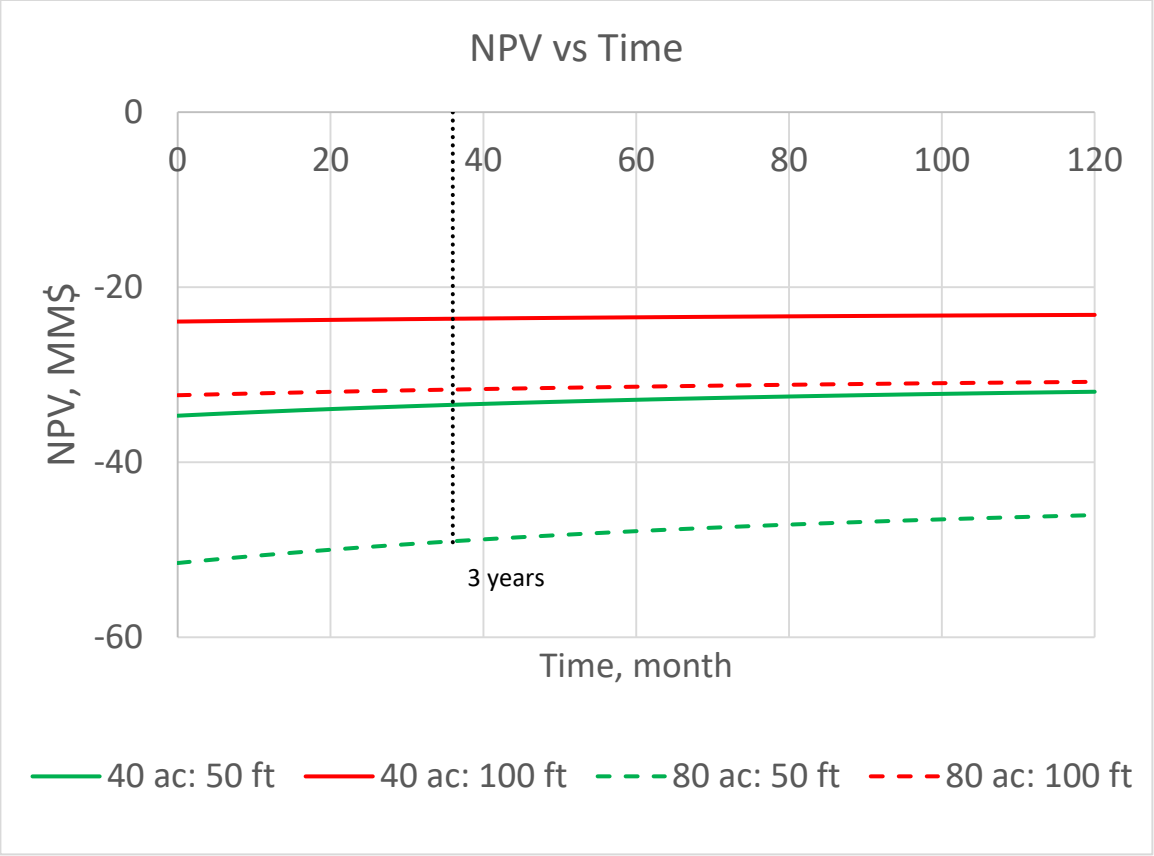

Figure 4.10. Barnett shale NPV estimation.

The analysis of the results presented in Figure 4.9 and 4.10 shows the same production trends in relation to the well and fracture spacing as were observed in the example for Eagle Ford. However, the reservoir is so tight (50 nd) that the well pattern cannot provide the rate that could be economical in 3 year period. Even the increase of the permeability to one order of magnitude will not make any of given configurations economical. With currently used input parameters from Table 4.7 the application of the proposed pattern in Barnett shale does not seem to be economical.

4.2.3 Bakken shale

The Bakken shale is primarily an oil play. It straddles the US border with Canada and runs through two states – North Dakota and Montana – and two Canadian provinces – Saskatchewan and Manitoba as shown in Figure 4.11. The US Geological Survey estimates there are 3.65 billion barrels of recoverable crude oil in Bakken, which would make it the largest oil field in the US outside Alaska (OGJ 2016a).

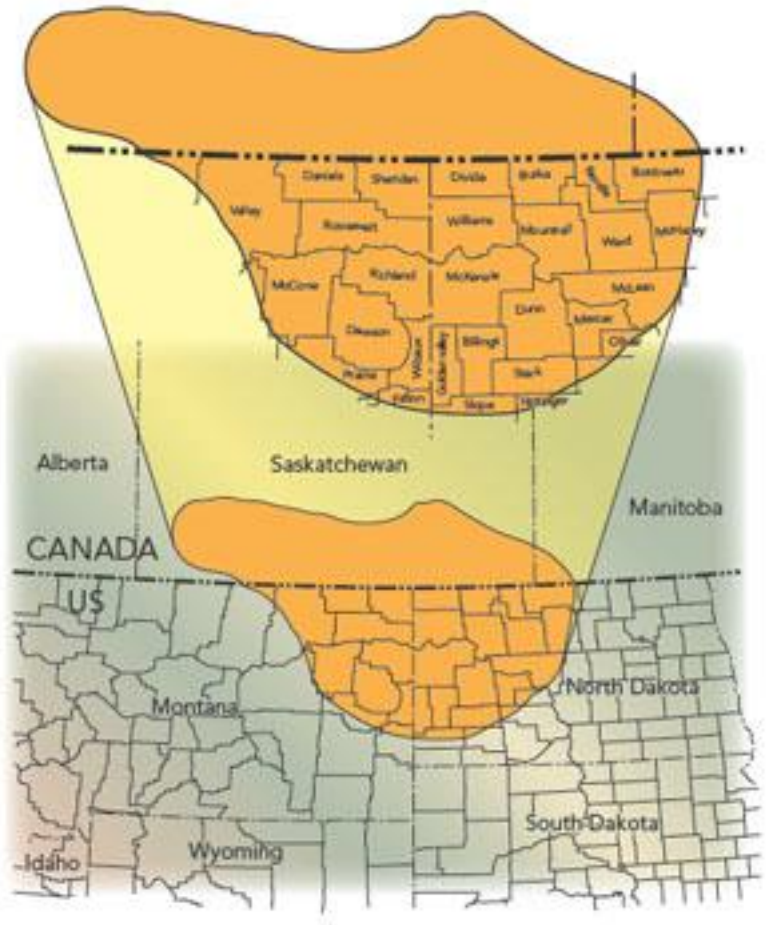

Figure 4.11. Bakken shale location map.

Bakken shale primarily consists of three major zones. In the upper and lower shale, the permeability is in nanodarcies. In the middle Bakken, it is presumably high in the rage of 0.001 – 0.1 md. The middle Bakken is the primary target of oil production with the average thickness of 100 ft and this zone will be considered for application of designed pattern.

The summary of estimated Bakken shale properties is given in Table 4.9 and based on the number of research publication such as Tran, Sinurat and Wattenbarger (2011), Kumar, Hoffman and Prasad (2013), Hoffman and Evans (2016), Flannery and Kraus (2006), Kuhlman, Perez and Claiborne (1992).

Table 4.9. Bakken shale input parameters.

Parameter	**Symbol**	**Value**
Rock and Fluid Properties		
Porosity, fraction	$ø$	0.05
Permeability, md	k	0.01
Oil viscosity, cp	μ_o	0.55
Water viscosity, cp	μ_w	0.43
Water Salinity, wt. %	S	6
Relative Permeability (Corey)		
Water Corey exponent	n_w	4
Oil Corey exponent	n_o	4
Connate water saturation, fraction	S_{wc}	0.25
Residual oil saturation, fraction	S_{or}	0.25
Water relative permeability at residual oil saturation	$k_{rw}(S_{or})$	0.45
Oil relative permeability at connate water saturation	$k_{ro}(S_{wc})$	1
Initial Reservoir Pressure and Bubble Point Pressure		
Reservoir depth (mid oil column), ft	H	10,000
Initial reservoir pressure, psia	p_i	4,515
Reservoir temperature, F	T	212
Vazquez & Beggs correlations		
Separator pressure, psia	p_{sep}	400
Separator temperature, F	T_{sep}	100
Gas specific gravity (p_{sep}, T_{sep})	γ_{gp}	0.78

Table 4.9 (continued).

Oil API gravity	API	40
Solution GOR, scf/STB	R_s	1,570
Bubble point pressure, psi	p_{bp}	4,457
Oil FVF, bbl/STB	B_o	1.5
Water FVF, bbl/STB	B_w	1
Minimum Horizontal Stress		
Rock density, lb/ft3	ρ	165
Poisson Ration	υ	0.3
Absolute minimum horizontal stress, psi	σ_{hmin}	6,768
Waterflood Constraints		
Injection pressure safety factor, psi	p_{injs}	50
Maximum injection pressure, psi	p_{inj}	6,718
Maximum I-P pressure drop, psi	$\Delta_{pI\text{-}P}$	2,261
Fracture properties		
Dimensionless infinite fracture conductivity	C_{fD}	50
Specific gravity of proppant material	ρ_{prop}	2.65
Porosity of proppant pack, fraction	ϕ_f	0.38
Proppant pack permeability, md	k_f	150,000
Max proppant diameter, inch	D_{pmax}	0.031
Economic parameters		
Vertical well construction cost, $/ft	C_{wv}	250
Horizontal well construction cost, $/ft	C_{wh}	500
Pumping charges, $/frac	C_{pump}	30,000
Proppant cost (20/40 ceramic, 150 Darcy), $/lbm	C_{prop}	1.5
Annual discount rate, fraction	r	0.1
Oil market price, $/STB	P	50

The compared pattern geometries are shown in Table 4.10.

Table 4.10. Bakken assessed pattern geometries.

Dimensions	**Cases (A_w: $x_{s(I\text{-}P)}$)**			
	40 ac: 50 ft	**40 ac: 100 ft**	**80 ac: 50 ft**	**80 ac: 100 ft**
Distance between I-P fractures, ft	50	100	50	100
Fracture height, ft	100	100	100	100
½ Fracture length, ft	165	165	330	330
Horizontal well length, ft	5,280	5,280	5,280	5,280

The oil rate and net present value estimations for Middle Bakken input parameters and different pattern geometries are shown in Figure 4.12 and 4.13.

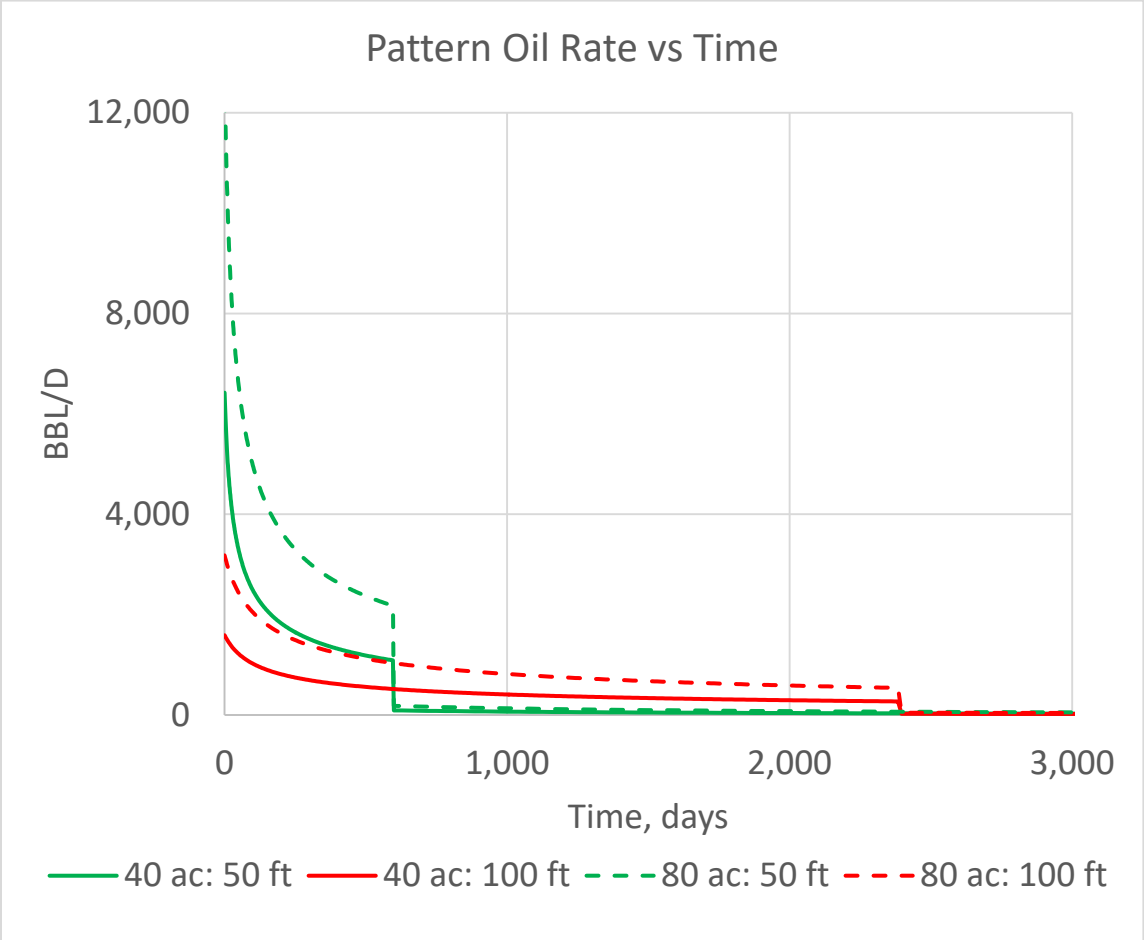

Figure 4.12. Bakken shale production oil rate estimation.

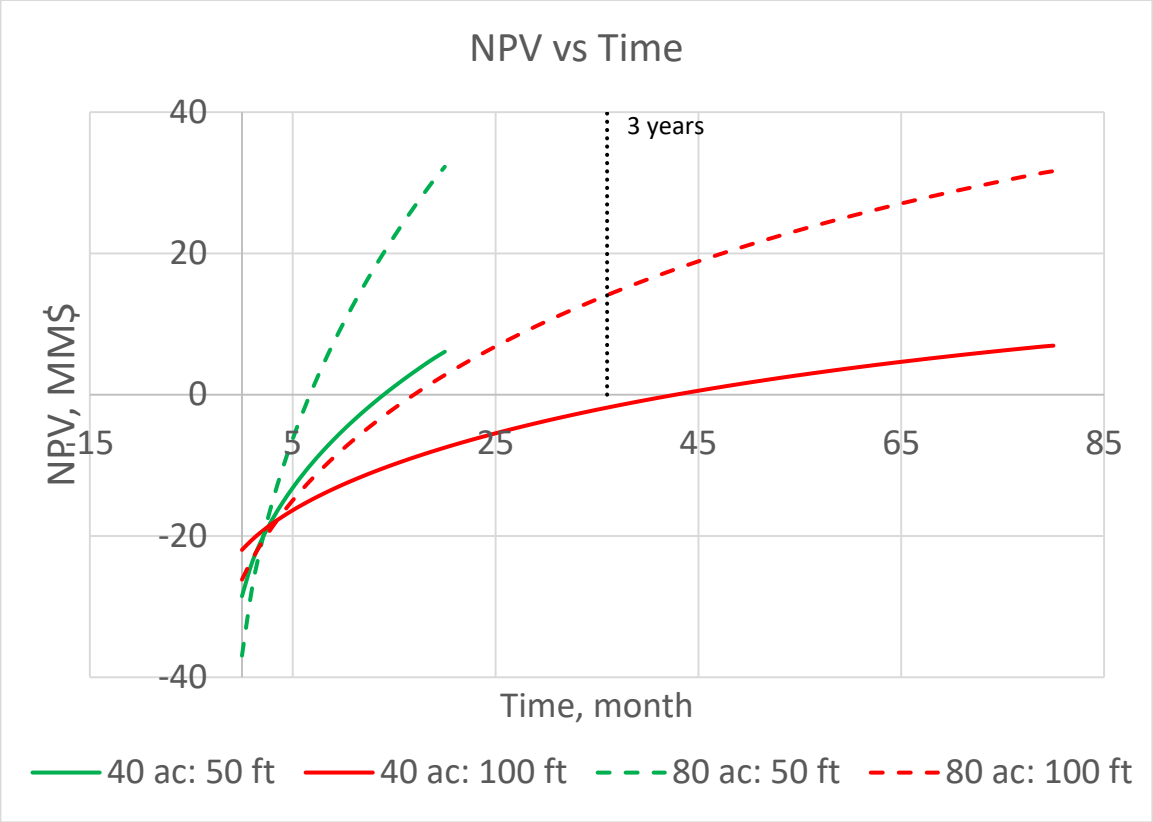

Figure 4.13. Bakken shale NPV estimation.

The analysis of the results presented in Figure 4.12 and 4.13 shows the same production trends in relation to the well and fracture spacing as were observed in the previous examples. The relatively high reservoir permeability allows the water to arrive into the production well (fracture) as early as in 20 months for the cases with I-P spacing of 50 ft and it takes about 6.5 years for the cases with 100 ft spacing. Economics shows that most configurations of the well pattern have positive NPV with the highest value of 32.3 MM$ for the production area of 80 ac and 50 ft I-P spacing. Thus, we can conclude that the designed pattern is a viable option for enhanced oil recovery in Bakken shale formation that can be economically applied.

4.2.4 Permian basin

According to RRC (2013), the Permian Basin is an oil and gas producing area located in West Texas and the adjoining area of southeastern New Mexico. The Permian Basin covers an area approximately 250 miles wide and 300 miles long and includes three basins: Delaware, Central Bain Platform, and Midland (see Figure 4.14). Various producing formations such as the Yates, San Andres, Clear Fork, Spraberry, Wolfcamp, Yeso, Bone Spring, Avalon, Canyon, Morrow, Devonian, and Ellenberger are all part of the Permian Basin, with oil and natural gas production ranging from depths from a few hundred feet to five miles below the surface.

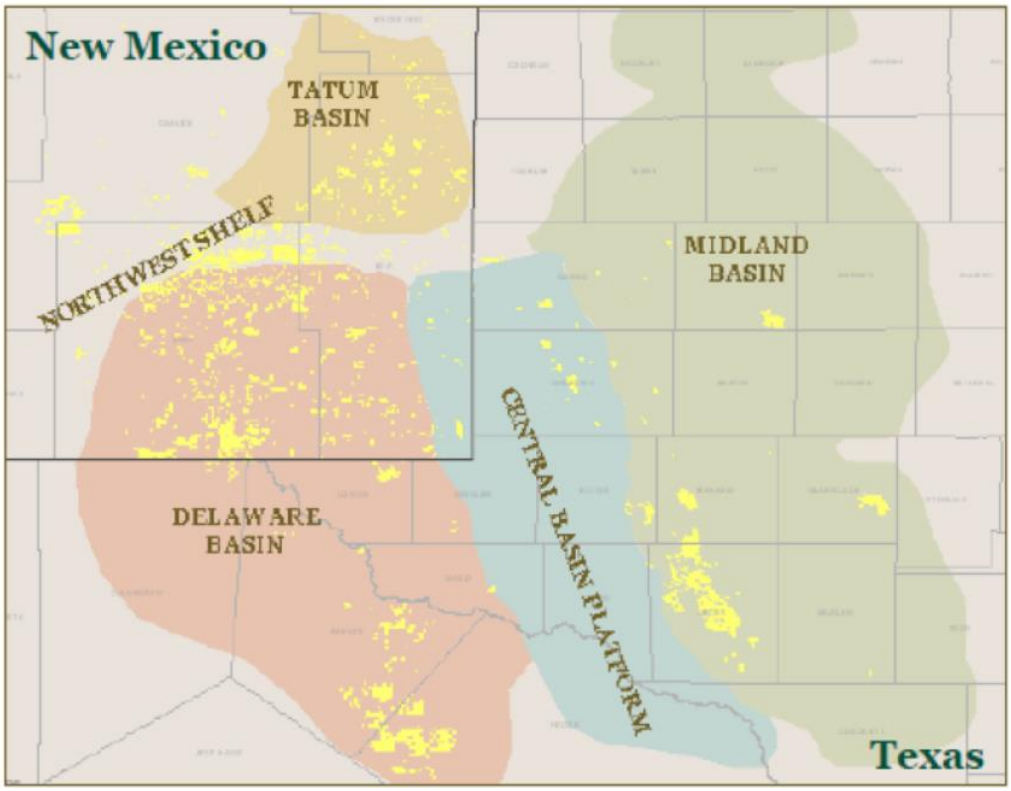

Figure 4.14. Permian Basin location map.

Although oil production has previously come from the more permeable portions of the Permian formations developed with vertical single stage fractured wells, the application of horizontal drilling and hydraulic fracturing has opened up large and less permeable portions of these formations to commercial production such as Wolfcamp. Because the Wolfcamp zone is omnipresent across all of the various basins comprise the Permian (Kelly et al., 2012), its characteristics will be used for assessing the application of the designed well pattern.

The Wolfcamp zone in Midland Basing has been a subject of study for many researchers such as Walls and Morcote (2015), Kelly et al. (2012), Mavor (2014), Rafatian and Capsan (2014). They indicated the massive net pay thickness of the Wolfcamp zone averaging about 600 ft with the average porosity about 10% and permeability in the range of 20 – 8000 nd with the average below 1000 nd. The summary of estimated Wolfcamp shale properties is given in Table 4.11.

Table 4.11. Permian Basin (Wolfcamp) input parameters.

Parameter	Symbol	Value
Rock and Fluid Properties		
Porosity, fraction	ϕ	0.1
Permeability, md	k	0.001
Oil viscosity, cp	μ_o	0.64
Water viscosity, cp	μ_w	0.57
Salinity, wt. %	S	6
Relative Permeability (Corey)		
Water Corey exponent	n_w	4
Oil Corey exponent	n_o	4
Connate water saturation, fraction	S_{wc}	0.25
Residual oil saturation, fraction	S_{or}	0.25
Water relative permeability at residual oil saturation	$k_{rw}(S_{or})$	0.45
Oil relative permeability at connate water saturation	$k_{ro}(S_{wc})$	1

Table 4.11 (continued).

Initial Reservoir Pressure and Bubble Point Pressure		
Reservoir depth (mid oil column), ft	H	7,000
Initial reservoir pressure, psia	p_i	3,450
Reservoir temperature, F	T	150
Vazquez & Beggs correlations		
Separator pressure, psia	p_{sep}	400
Separator temperature, F	T_{sep}	100
Gas specific gravity (p_{sep}, T_{sep})	γ_{gp}	0.78
Oil API gravity	API	39
Solution GOR, scf/STB	R_s	700
Bubble point pressure, psi	p_{bp}	2,281
Oil FVF, bbl/STB	B_o	1.35
Water FVF, bbl/STB	B_w	1
Minimum Horizontal Stress		
Rock density, lb/ft3	ρ	165
Poisson Ration	υ	0.3
Absolute minimum horizontal stress, psi	σ_{hmin}	4,857
Waterflood Constraints		
Injection pressure safety factor, psi	p_{injs}	50
Maximum injection pressure, psi	p_{inj}	4,807
Maximum I-P pressure drop, psi	$\Delta_{pI\text{-}P}$	2,526
Fracture properties		
Dimensionless infinite fracture conductivity	C_{fD}	50
Specific gravity of proppant material	ρ_{prop}	2.65
Porosity of proppant pack, fraction	ϕ_f	0.38
Proppant pack permeability, md	k_f	150,000
Max proppant diameter, inch	D_{pmax}	0.031
Economic parameters		
Vertical well construction cost, $/ft	C_{wv}	250
Horizontal well construction cost, $/ft	C_{wh}	500
Pumping charges, $/frac	C_{pump}	30,000
Proppant cost (20/40 ceramic, 150 Darcy), $/lbm	C_{prop}	1.5
Annual discount rate, fraction	r	0.1
Oil market price, $/STB	P	50

The compared pattern geometries are shown in Table 4.12.

Table 4.12. Permian Basin (Wolfcamp) assessed pattern geometries.

Dimensions	Cases (A_w: $x_{s(I-P)}$)			
	40 ac: 50 ft	40 ac: 100 ft	80 ac: 50 ft	80 ac: 100 ft
Distance between I-P fractures, ft	50	100	50	100
Fracture height, ft	600	600	600	600
½ Fracture length, ft	165	165	330	330
Horizontal well length, ft	5,280	5,280	5,280	5,280

The oil rate and net present value estimations for Wolfcamp input parameters and different pattern geometries are shown in Figure 4.15 and 4.16.

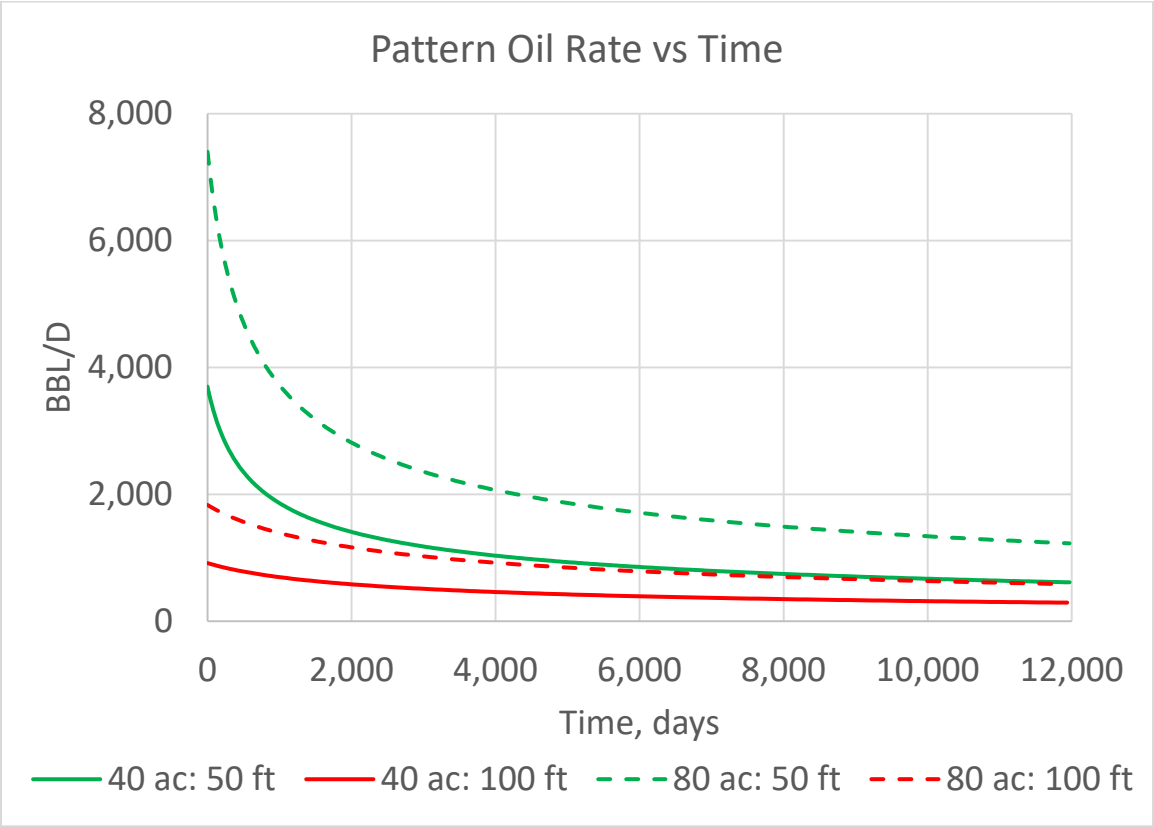

Figure 4.15. Permian Basin (Wolfcamp) production oil rate estimation.

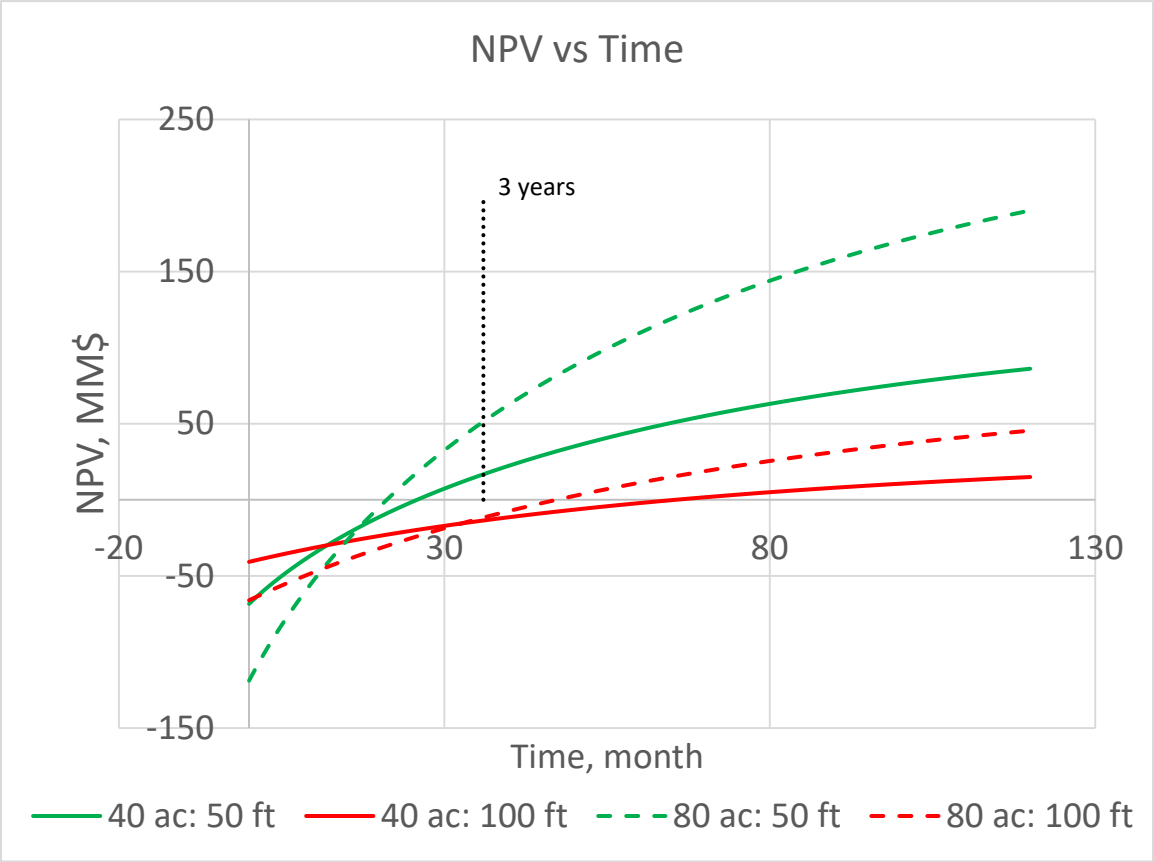

Figure 4.16. Permian Basin (Wolfcamp) NPV estimation.

The analysis of the results presented in Figure 4.15 and 4.16 shows the same production trends in relation to the well and fracture spacing as were observed in the previous examples. The large net pay thickness and not very low reservoir permeability allow for quite high initial oil rates and positive economics at the end of 3-year production period for cases with I-P fracture spacing of 50 ft. Based on that, we can conclude that the designed pattern is a viable option for enhanced oil recovery in Permian Basin and specifically in Wolfcamp formation.

4.3 Chapter summary

In this chapter, the analytical screening tool was used to investigate the performance of the designed pattern at different geometries and reservoir conditions. In general, the larger the well spacing and the smaller the I-P fracture spacing the better performance could be expected. The reservoir permeability has a tremendous effect on the well pattern performance – the higher the permeability the proportionally better oil rate could be expected. The economics of well pattern depends on the production oil rate and initial investments. The initial investments include wells construction cost and the cost of the stimulation where the main variable in our cases is the amount of the proppant needed to have the infinite fracture conductivity. The higher the reservoir permeability the higher volume of proppant is needed.

The sensitivity runs of the designed pattern were completed on the major US shale plays using the publicly available reservoir and fluid properties. The summary of these runs is shown in Table 4.13 and indicates that proposed well pattern design could be applicable in Eagle Ford, Bakken, and Permian formations. The sensitivity runs performed for Barnett shale shows that low reservoir permeability prevents the designed well pattern for waterflood to be successful in this formation.

Table 4.13. Summary of sensitivity runs for the major US shale plays.

Waterflood KPI	Cases (A_w: $x_{s(I-P)}$)			
	40 ac: 50 ft	**40 ac: 100 ft**	**80 ac: 50 ft**	**80 ac: 100 ft**
Eagle Ford shale				
Water breakthrough time, days	6,208	24,833	6,208	24,833
Initial (max) oil production rate per reservoir unit, bbl/d	8.7	4.4	17.5	8.7
Initial (max) oil production rate per pattern, bbl/d	3,649	907	7,297	1,814
NPV @ BT or NPV @ 3 years, MM$	9.8	-9.2	39.6	-0.7
Middle Bakken shale				
Water breakthrough time, days	598	2,395	598	2,395
Initial (max) oil production rate per reservoir unit, bbl/d	15.3	7.7	30.6	15.3
Initial (max) oil production rate per pattern, bbl/d	6,248	1,579	12,495	3,158
NPV @ BT or NPV @ 3 years, MM$	6.1	-1.8	32.3	14.1
Permian Basin (Wolfcamp)				
Water breakthrough time, days	13,787	55,145	13,787	55,145
Initial (max) oil production rate per reservoir unit, bbl/d	8.8	4.4	17.6	8.8
Initial (max) oil production rate per pattern, bbl/d	3,694	916	7,388	1,831
NPV @ BT or NPV @ 3 years, MM$	16.8	-13.6	51.4	-11.7
Barnett shale				
Water breakthrough time, days	325,070	1,300,282	325,070	1,300,282
Initial (max) oil production rate per reservoir unit, bbl/d	0.12	0.06	0.23	0.12
Initial (max) oil production rate per pattern, bbl/d	49	12	97	24
NPV @ BT or NPV @ 3 years, MM$	-33.4	-23.6	-49	-31.7

CHAPTER 5 CONCLUSIONS AND RECOMMENDATIONS

The objective of this study was to design a well pattern using MTFHWs that can optimize recovery of tight oil during waterflood and confirm whether this well pattern can be used economically in the major US shale plays. We have explained why existing well patterns are not optimally designed to perform secondary recovery of oil in the tight formations and suggested reasons for reported unsuccessful waterflood field trials.

The proposed well pattern mitigates the disadvantages of the existing well patterns and provides the most efficient 1-D “plane-to-plane” waterflood performance. An analytical screening tool based on well-known Buckley-Leverett method was developed to assess the performance of the proposed well pattern. The Buckley-Leverett method gives a good estimate of the best performance that will ever be observed and in comparison to the modern simulation technique is very quick and requires fewer input data. If the analytical screening tool suggests that a given well scenario is uneconomical, the need for more complicated reservoir simulations is unlikely, since the performance will only be worse.

In the course of this research, it was found that the waterflood together with the application of the suggested well pattern in Eagle Ford, Bakken, and Permian formations could be potentially economical. The wider well spacing and tighter hydraulic fracture spacing increase the production rate and improve the economics of the project. In contrast, the implementation of the waterflooding in Barnett shale seems to be uneconomical due to very low reservoir permeability.

In the case when the described well pattern and analytical screening tool indicate potential economical waterflood in the particular formation the other tools, such as reservoir simulation, should be used to account for impacts of additional aspects including reservoir heterogeneity, natural fracture network, three-phase flow, compressibility, and primary production.

Ideas for further work include the following:

The performance of the proposed well pattern could potentially be hurt by the high permeability streaks or active natural fracture network that could short circuit the water injection and leave behind upswept areas. Research in the use of different emulsions or calcite-producing bacteria to improve flow conformance is suggested.

Finally, the author of this research understands that operational difficulties in implementation of the proposed pattern design could lead to the disappointing outcome. That is why the extra research is suggested in the areas of fracture detection and isolation.

REFERENCES

Andersen, S.A., Hansen, S.A., and Fjeldgaard K. 1988. "Horizontal Drilling and Completion: Denmark." Article SPE-18349-MS. http://dx.doi.org/10.2118/18349-MS

Arthur, J. D., Bohm, B., and Layne, M. 2008. "Hydraulic Fracturing Considerations for Natural Gas Well of the Marcellus Shale." Article presented at the Ground Water Protection Council 2008 Annual Forum, Cincinnati, Ohio, 21-24 September.

Awada, A., Santo, M., Lougheed, D., Xu, D., Virues, C. 2016. "Is That Interference? A Work Flow for Identifying and Analyzing Communication Through Hydraulic Fractures in a Multiwell Pad." Article SPE-178509-PA. http://dx.doi.org/10.2118/178509-PA

Biot, M. A., 1956. "General Solutions of the Equations of Elasticity and Consolidation for a Porous Material." *Journal of Applied Mechanics*, Vol. 23.

Braun, D., Powell, B., Guo, R., Morad, K., Flint, D., Dixon, R. K. 2014. "Entering a Liquid-Rich Shale Play Near the Top of the Learning Curve: Early Quantification and Application of Development Best Practices." Article SPE-171658-MS. http://dx.doi.org/10.2118/171658-MS

Buckley, S. E. and Leverett, M. C. 1942. "Mechanism of Fluid Displacement in Sands." Article SPE-942107-G. http://dx.doi.org/10.2118/942107-G

Bybee, K. 2007. "Optimizing Completion Strategies for Fracture Initiation in Barnett Shale Horizontal Wells." Article SPE-0307-0045-JPT. http://dx.doi.org/10.2118/0307-0045-JPT

Cipolla, C. L., Lolon, E, and Mayerhofer, M. J. 2009. "Resolving Created, Propped, and Effective Hydraulic-Fracture Length." Article SPE-129618-PA. http://dx.doi.org/10.2118/129618-PA

Cipolla, C.L., Lolon, E.P., Erdle, J.C., Rubin, B. 2010. "Reservoir Modeling in Shale-Gas Reservoirs." Article SPE-125530-MS. http://dx.doi.org/10.2118/125530-pa

Corey, A. T. 1954. "The Interrelation Between Gas and Oil Relative Permeability." *Producers monthly*, 19(1), 38-41.

Craig, F. F. 1971. The Reservoir Engineering Aspects of Waterflooding. Second printing. SPE of AIME. Dallas, Tx: Millet.

Crosby, D. G., Yang, Z., and Rahman, S. S. 1998. "Transversely Fractured Horizontal Wells: A Technical Appraisal of Gas Production in Australia." Article SPE-50093-MS. http://dx.doi.org/10.2118/50093-MS

Economides, M. J., and Nolte, K. G. 2000. Reservoir Stimulation. Third edition. Chichester: Wiley & Sons.

EIA. 2013. “Technically Recoverable Shale Oil and Shale Gas Resources: An Assessment of 137 Shale Formations in 41 Countries Outside the United States.” Article. US Energy Information Administration, Washington, D.C.

EIA. 2015a. “World Shale Resource Assessments.” Article. US Energy Information Administration. http://www.eia.gov/analysis/studies/worldshalegas/

EIA. 2015b. “Annual Energy Outlook 2015.” Article. US Energy Information Administration, Washington, D.C.

Flannery, J., and Kraus, J. 2006. “Integrated Analysis of the Bakken Petroleum System.” Article. U.S. Williston Basin 2006 AAPG Bulletin. http://www.searchanddiscovery.net/documents/2006/06035flannery/index.htm (last accessed on 15 July 2016).

Foster, J. 2014. “Applying Technology to Enhance Unconventional Shale Production.” Article SPE-1214-0018-JPT. http://dx.doi.org/10.2118/1214-0018-JPT

Frantz, J. H., Sawyer, W. K., MacDonald, R. J., Williamson, J. R., Johnston, D., Waters, G. 2005. “Evaluating Barnett Shale Production Performance-Using an Integrated Approach.” Article SPE-96917-MS. http://dx.doi.org/10.2118/96917-MS

Gong, X., Tian, Y., McVay, D. A., Ayers, W. B, Lee, J. 2013. “Assessment of Eagle Ford Shale Oil and Gas Resources.” Article SPE-167241-MS. http://dx.doi.org/10.2118/167241-MS

Hayes, H. J. 1976. Enhanced Oil Recovery. Natl. Pet. Council, Washington, D.C.

Hoffman, B. T. and Evans, J. G. 2016. "Improved Oil Recovery IOR Pilot Projects in the Bakken Formation." Article SPE-180270-MS. http://dx.doi.org/10.2118/180270-MS

Honarpour, M. M., Nagarajan, N. R., Orangi, A., Arasteh, F., Yao, Z. 2012. "Characterization of Critical Fluid PVT, Rock, and Rock-Fluid Properties - Impact on Reservoir Performance of Liquid Rich Shales." Article SPE-158042-MS. http://dx.doi.org/10.2118/158042-MS

Huang, W. S., Kaetzer, T. R., and Bowlin, K.R. 1996. "Waterflooding in a Tight Sandstone Reservoir with Horizontal Injector and Producer at New Hope Shallow Unit Texas." Article PETSOC-96-02-06. http://dx.doi.org/10.2118/96-02-06

Hubbert, M. K., and Willis, D. G. 1957. "Mechanics Of Hydraulic Fracturing." Article SPE-686-G.

Jacobs, T. 2016. "EOR for Shale: Ideas to Boost Output." *Journal of Petroleum Technology*, June 2016, 28-31.

Kale, S. V., Rai, C. S., and Sondergeld C. H. 2010. "Petrophysical Characterization of Barnett Shale." Article SPE-131770-MS. http://dx.doi.org/10.2118/131770-MS

Kelly, L., Bachmann, J., Amoss, D., Angelico, B., Corales, B., Femandez, B., Kissel, P., Roberts, R., Stewart, H. 2012. "Permian Basin: Easy to Oversimplify, Hard to Overlook." *Exploration and Production*, January 19, 2012.

Kuhlman, R.D., Perez, J.I., and Claiborne, E.B. 1992. "Microfracture Stress Tests, Anelastic Strain Recovery, and Differential Strain Analysis Assist in Bakken Shale Horizontal Drilling Program." Article SPE-24379-MS. http://dx.doi.org/10.2118/24379-MS

Kumar, S., Hoffman, T., and Prasad P. 2013. "Upper and Lower Bakken Shale Production Contribution to the Middle Bakken Reservoir." Article SPE-168797-MS. http://dx.doi.org/10.1190/URTEC2013-001

Lawal, H., Jackson, G., Abolo, N., Flores, C. 2013. "A Novel Approach To Modeling and Forecasting Frac Hits In Shale Gas Wells." Article SPE-164898-MS. http://dx.doi.org/10.2118/164898-MS

Mavor, M. 2014. "Reservoir Fluid Properties Required for Low-Permeability Oil Reservoir Analysis." *Search and Discovery,* March 10, 2014.

Miller, B. A., Paneitz, J. M., Yakeley, S., Evans, K. A. 2008. "Unlocking Tight Oil: Selective Multistage Fracturing in the Bakken Shale." Article SPE-116105-MS. http://dx.doi.org/10.2118/116105-MS

Montgomery, S. L., Jarvie, D.M., Bowker, K. A., Pollastro, R. M. 2005. "Mississippian Barnett Shale, Fort Worth Basin, North Central Texas: Gas-shale play with multi–trillion cubic foot potential." *AAPG Bulletin*, v. 89, p. 155–175.

Morsy, S., Sheng, J. J., and Ezewu, R. O. 2013. "Potential of Waterflooding in Shale Formations." Article SPE-167510-MS. http://dx.doi.org/10.2118/167510-MS

Morsy, S., Sheng, J. J., and Soliman, M. Y. 2013. "Waterflooding in the Eagle Ford Shale Formation: Experimental and Simulation Study." Article SPE-167056-MS. http://dx.doi.org/10.2118/167056-MS

Mukherjee, H. and Economides, M.J. 1991. "A Parametric Comparison of Horizontal and Vertical Well Performance." Article SPE-18303-PA. http://dx.doi.org/10.2118/18303-PA

Mullen, J., Lowry, J. C., and Nwabuoku, K.C. 2010. "Lessons Learned Developing the Eagle Ford Shale." Article SPE-138446-MS. http://dx.doi.org/10.2118/138446-MS

Nieto, J., Bercha, R., and Chan, J. 2009. "Shale Gas Petrophysics - Montneyand Muskwa, Are They Barnett Look-Alikes?" Article held jointly by the Society of Petrophysicists and Well Log Analysts (SPWLA). SPWLA-2009-84918.

OGJ. 2016a. "Bakken Shale." Article. http://www.ogj.com/unconventional-resources/bakken-shale.html?cmpid=UOGRtopNav (last accessed on July 15).

OGJ. 2016b. "Barnett Shale." Article. http://www.ogj.com/unconventional-resources/barnett-shale.html?cmpid=UOGRtopNav (last accessed on July 15).

OGJ. 2016c. "Eagle Ford Shale." Article. http://www.ogj.com/unconventional-resources/eagle-ford-shale.html?cmpid=UOGRtopNav (last accessed on July 15).

Rafatian, N. and Capsan, J. 2014. “Petrophysical Characterization of the Pore Space in Permian Wolfcamp Rocks.” Article SPWLA-2014-X. Society of Petrophysicists and Well-Log Analysts, May 2014.

Rankin, R. R., Thibodeau, M., Vincent, M. C., and Palisch, T. T. 2010. “Improved Production and Profitability Achieved with Superior Completions in Horizontal Wells: A Bakken/Three Forks Case History.” Article SPE-134595-MS. http://dx.doi.org/10.2118/134595-MS

RRC. 2013. “Permian Basin Information.” Article. http://www.rrc.state.tx.us/oil-gas/major-oil-gas-formations/permian-basin/ (last accessed on July 20).

Sandhu K. 2011. “Secondary and Tertiary Recovery from Tight Oil Reservoir.” Article Gaffney, Cline & Associates. https://www.uwyo.edu/eori/_files/eor_ior_jackson_12/kerry%20-%20ior%20and%20eor%20of%20tight%20oil%20reservoirs.pdf (last accessed on 18 June 2016)

Soliman, M. Y., Hunt, J. L, and El Rabaa, A. M. 1990. “Fracturing Aspects of Horizontal Wells.” Article SPE-18542-PA. http://dx.doi.org/10.2118/18542-PA

Tehrani, A.D.H. 1992. “An Overview of Horizontal Well Targets Recently Drilled in Europe.” Article SPE-22390-MS. http://dx.doi.org/10.2118/22390-MS

Terwilliger, P. L., Wilsey, L. E., Hall, H. N., Bridges, P. M., and Morse, R. A. 1951. "An Experimental and Theoretical Investigation of Gravity Drainage Performance." *AIME*, 192, 285-296.

Thomas, A., Kumar, A., Rodrigues, K., Sinclair, R. I., Lackie, C., Galipeault, A., and Blair, M. 2014. "Understanding Water Flood Response in Tight Oil Formations: A Case Study of the Lower Shaunavon." Article SPE-171671-MS. http://dx.doi.org./10.2118/171671-MS

Tran, T., Sinurat, P. D., and Wattenbarger B. A. 2011. "Production Characteristics of the Bakken Shale Oil." Article SPE-145684-MS.

Vazuquez, M. and Beggs, H. D. 1980. "Correlation for Fluid Physical Property Prediction." Article SPE-6719-PA. http://dx.doi.org/10.2118/6719-PA

Walls, J. D. and Morcote, A. 2015. "Quantifying Variability of Reservoir Properties from a Wolfcamp Formation Core." Article SPE-178601-MS. http://dx.doi.org/10.2118/178601-MS

Welge, H. J. 1952. "A Simplified Method for Computing Oil Recovery by Gas or Water Drive." *AIME,* 195, 91-98.

Whitson, C. H. and Sunjerga, S. 2012. "PVT in Liquid-Rich Shale Reservoirs." Article SPE-155499-MS. http://dx.doi.org/10.2118/155499-MS

Willhite, G.P. 1986. Waterflooding. SPE Textbook Series vol. 3, Richardson, Tx: SPE.

Wolcott, D. 2009. Applied Waterflooding. Hoston, TX: Energy Tribune Publishing.

Yang, T., Basquet, R., Callejon, A., Joost Van Roosmalen, J., Bartusiak, B. 2014. "Shale PVT Estimation Based on Readily Available Field Data." Article SPE-2014-1884129-MS. http://dx.doi.org/10.15530/urtec-2014-1884129

Yost, A. B. and Overby, W. K. 1989. "Production and Stimulation Analysis of Multiple Hydraulic Fracturing of a 2000 ft Horizontal Well." Article SPE-19090-MS. http://dx.doi.org/10.2118/19090-MS

Zwahlen, E. and Patzek, T. W. 1997. "Linear Transient Flow Solution for Primary Oil Recovery with Infill and Conversion to Water Injection." Article SPE-38290-MS. http://dx.doi.org/10.2118/38290-MS

Beggs, H. D., Robinson, J. R. 1975. "Estimating the Viscosity of Crude Oil Systems." Article SPE-5434-PA. http://dx.doi.org/10.2118/5434-PA

McCain, W. D. 1991. "Reservoir-Fluid Property Correlations-State of the Art (includes associated papers 23583 and 23594)." Article SPE-18571-PA. http://dx.doi.org/10.2118/18571-PA

APPENDIX A INPUT SCREEN OF THE ANALITICAL SCREENING TOOL

Data for Rate Calculation at Constant Pressure Drop — PLEASE CHANGE DATA ONLY IN GREEN CELLS

Rock and Fluid Properties		Manual Input	Estimation
Porosity, fraction	ø	0.085	
Permeability, md	k	0.00080	
Wettability	0 (water wet) to 1 (oil wet)	0.5	
Oil viscosity, cp	μ_o	0.4	0.4
Water viscosity, cp	μ_w	0.2	0.2
Water salinity, wt. %	S	6.0	

Relative Permeability (Corey)		Manual Input	Estimation
Water Corey exponent	n_w	4	4.00
Oil Corey exponent	n_o	4	4.00
Connate water saturation, fraction	S_{wc}	0.25	0.25
Residual oil saturation, fraction	S_{or}	0.25	0.25
Water relative permeability at residual oil saturation	$k_{rw}(S_{or})$	0.45	0.45
Oil relative permeability at connate water saturation	$k_{ro}(S_{wc})$	1	1.00

Initial Reservoir Pressure and Bubble Point Pressure		Manual Input	Estimation
Reservoir depth (mid oil column), ft	H	10,000	
Initial reservoir pressure, psia	p_i	5,000	5,000
Reservoir temperature, F	T	244	244
Vazquez & Beggs correlations			
Separator pressure, psia	p_{sep}	400	
Separator temperature, F	T_{sep}	100	
Gas specific gravity (p_{sep}, T_{sep})	γ_g	0.78	
Oil API gravity	API	42.1	
Solution GOR, scf/STB	R_s	1,007	1,007
Bubble point pressure, psi	p_{bp}		3,342
Oil FVF, bbl/STB	B_o		1.5
Water FVF, bbl/STB	B_w	1	

Min Horizontal Stress		Manual Input	Estimation
Rock density, lb/ft3	ρ_r	165	
Poisson Ration	υ	0.3	
Absolute minimum horizontal stress, psi	σ_{hmin}		6,968

Waterflood Constraints		Case1	Case2	Case3	Case4
Injection pressure safety factor, psi	p_{injs}	50	50	50	50
Maximum injection pressure, psi	p_{inj}	6,918	6,918	6,918	6,918
Maximum I-P pressure drop, psi	Δp_{I-P}	3,575	3,575	3,575	3,575

Reservoir Unit Dimensions		Case1	Case2	Case3	Case4
Distance between I-P fractures, ft	$x_{s(I-P)}$	50	100	200	300
Fracture height, ft	h_f	250	250	250	250
½ Fracture length, ft	x_f	150	150	150	150

Oil Production		Case1	Case2	Case3	Case4
Water breakthrough time, days	t_{BT}	4,438	17,754	71,018	159,790
Initial (max) oil production rate per reservoir unit, bbl/	q	6.04	3.02	1.51	1.01
Initial (max) oil production rate per pattern, bbl/d	q_T	2,533	628	157	68
NPV @ BT or NPV @ 3 years, MM$	NPV	**8.3**	**-11.5**	**-16.8**	**-17.0**

Data for Economic Calculations

Calculate

Pattern Geometry		Case1	Case2	Case3	Case4
Horizontal well length, ft	L_w	5,280	5,280	5,280	5,280

Fracture Properties		
Dimensionless infinite fracture conductivity	C_{fD}	50
Specific gravity of proppant material	ρ_{srop}	2.65
Porosity of proppant pack, fraction	ϕ_f	0.38
Proppant pack permeability, md	k_f	150,000
Max proppant diameter, inch	D_{pmax}	0.031

Economic Parameters		
Vertical well construction cost, $/ft	C_{wv}	250
Horizontal well construction cost, $/ft	C_{wh}	500
Pumping charges, $/frac	C_{pump}	30,000
Proppant cost (20/40 ceramic, 150 Darcy), $/lbm	C_{prop}	1.5
Annual discount rate, fraction	r	0.1
Oil market price, $/STB	P	50

APPENDIX B EQUATIONS AND CORRELATIONS USED FOR DEFAULT VALUES

Corey equations for relative permeability. For water

$$k_{rw} = k_{rw}(S_{or})\left(\frac{S_w - S_{wc}}{1 - S_{wc} - S_{or}}\right)^{n_w}$$

and for oil

$$k_{ro} = k_{ro}(S_{wc})\left(\frac{1 - S_w - S_{or}}{1 - S_{wc} - S_{or}}\right)^{n_o}.$$

Vazquez and Beggs correlations for bubble point pressure and solution GOR

$$R_s = C_1 \gamma_{gs} p_{sep}^{C_2} \exp\left(C_3 \frac{\gamma_{oAPI}}{T + 460}\right),$$

$$P_{bp} = \left[\left(\frac{A_1 R_s}{\gamma_{gs}}\right) \text{antilog}\left(-A_3 \frac{\gamma_{oAPI}}{T + 460}\right)\right]^{A_2},$$

where γ_{gs} – gas specific gravity that would result from separator condition of 100 psig and could be found as

$$\gamma_{gs} = \gamma_{gp}\left[1 + 5.912 \times 10^{-5} \gamma_{oAPI} T_{sep} \log\left(\frac{p_{sep}}{114.7}\right)\right].$$

Vazquez and Beggs correlations for oil FVF and oil compressibility

$$B_o = B_{ob} exp\left[c_o(p_{bp} - p_i\right],$$

where B_{ob} – oil FVF at bubble point pressure and could be calculated as

$$B_{ob} = 1 + D_1 R_s + D_2(T - 60)\left(\frac{\gamma_o}{\gamma_{gs}}\right) + D_3 R_s(T - 60)\left(\frac{\gamma_o}{\gamma_{gs}}\right),$$

and c_o – oil isothermal compressibility that can be estimated as

$$c_o = \frac{-1433 + 5R_s + 17.2T - 1180\gamma_{gs} + 12.61\gamma_o}{10^5 p}.$$

The coefficients *C*, *A*, and *D* depend on oil API gravity and listed in the table below.

Vazques and Beggs coefficient	Value	
	$\gamma_{oAPI} \leq 30$	$\gamma_{oAPI} > 30$
C_1	0.0362	0.0178
C_2	1.0937	1.187
C_3	25.724	23.931
A_1	27.64	56.06
A_2	1.0937	1.187
A_3	11.172	10.393
D_1	4.667×10^{-4}	4.67×10^{-4}
D_2	1.751×10^{-5}	1.1×10^{-5}
D_3	-1.811×10^{-8}	1.337×10^{-9}

Vazquez and Beggs correlation for oil viscosity

$$\mu_o = \mu_{ob}\left(\frac{p_i}{p_{bp}}\right)^m,$$

where parameter *m* is determined as

$$m = 2.6 p_i^{1.187} exp[-(11.513 + 8.98 * 10^{-5} p_i)].$$

Viscosity of oil at bubble point pressure (μ_{ob}) can be obtained from Beggs and Robinson correlations

$$\mu_{ob} = 10.715(R_s + 100)^{-0.515} \mu_{od}^{5.44(R_s+150)^{-0.338}},$$

where the dead oil viscosity (μ_{od}) could be estimated as

$$\mu_{od} = 10^X - 1,$$

where parameter *X* is

$$X = [10^{3.0324-0.02023\gamma_o}]T^{-1.163}.$$

Initial reservoir pressure calculated based on hydrostatic law and hydrostatic coefficient assumed equal to 0.45 psi/ft

$$p_i = 0.45H + 15.$$

Reservoir temperature calculated based on the geothermal coefficient assumed equal to 1.6 F/100 ft

$$T = \frac{H}{100 * 1.6}.$$

Absolute vertical stress could be estimated as

$$\sigma_v = \int_0^H \rho(H) g dH$$

and absolute minimum horizontal stress could be estimated as

$$\sigma_h = \frac{\nu}{1-\nu}\sigma_v + p\alpha\frac{1-2\nu}{1-\nu},$$

where *v* – Poisson's ration, *α* – Biot's poroelastic constant, a *p* – reservoir pressure.

APPENDIX C LINEAR WATERFLOOD AT CONSTANT PRESSURE DROP

The mobility ratio is

$$M = \frac{k_{rw}/\mu_w}{k_{ro}/\mu_o} = \frac{k_{rw}}{\mu_w}\frac{\mu_o}{k_{ro}}.$$

The endpoint mobility ratio is

$$M_e = \frac{k_{rw}(S_{or})/\mu_w}{k_{ro}(S_{wc})/\mu_o}.$$

In general, when $M_e < 1$ then the displacement process is a stable process – the oil is travelling with a velocity equal to, or greater than, that of the water which results in sharp interface between the fluids. When $M_e > 1$ then the displacement is not a stable process and oil will be by-passed by water resulting in water fingering.

The shock front mobility ratio is

$$M_{sf} = \frac{k_{ro}(S_{wf})/\mu_o + k_{rw}(S_{wf})/\mu_w}{k_{ro}(S_{wc})/\mu_o},$$

where S_{wf} – saturation at the Buckley-Leverett waterfront(shock front). If $M_{sf} < 1$ the displacement process is piston like, if $M_{sf} > 1$ then the fingering is likely at the waterfront into the oil zone.

Darcy equation for oil and water is

$$u_w = \frac{q_w}{A} = -\frac{Kk_{rw}(S_w)}{\mu_w}\left(\frac{dP}{dx} + \Delta\rho g \frac{dz}{dx} - P_c\right),$$

if α is the dip angle then

$$\frac{dz}{dx} = \sin\alpha\ .$$

If gravity and capillary forces are neglected the equation is

$$u_w = \frac{q_w}{A} = -\frac{Kk_{rw}(S_w)}{\mu_w}\left(\frac{dP}{dx}\right).$$

Thus the water and oil flow are proportional to

$$u_w = C\frac{k_{rw}(S_w)}{\mu_w}$$

and

$$u_o = C\frac{k_{ro}(S_w)}{\mu_o}.$$

The total flow rate is equal to

$$q_t = q_w + q_o.$$

Thus, the total velocity is equal to

$$u_t = u_w + u_o.$$

The fractional flow of water can be defined as

$$f_w = \frac{q_w}{q_w + q_o} = \frac{u_w}{u_w + u_o} = \frac{1}{1 + \frac{u_o}{u_w}}$$

or

$$f_w = \frac{1}{1 + \frac{k_{ro}(S_w)}{\mu_o} \frac{\mu_w}{k_{rw}(S_w)}}.$$

The slope of the fractional flow curve can be calculated as

$$\frac{df_w}{dS_w} = \frac{\frac{1}{\mu_w}\frac{dk_{rw}(S_w)}{dS_w}(u_w + u_o) - u_w\left(\frac{1}{\mu_w}\frac{dk_{rw}(S_w)}{dS_w} + \frac{1}{\mu_o}\frac{dk_{ro}(S_w)}{dS_w}\right)}{(u_w + u_o)^2},$$

where

$$\frac{k_{rw}(S_w)}{dS_w} = \frac{1}{1 - S_{wc} - S_{or}}\left(\frac{S_w - S_{wc}}{1 - S_{wc} - S_{or}}\right)^{n_w - 1} n_w k_{rw}(S_{or})$$

$$\frac{k_{ro}(S_w)}{dS_w} = \frac{-1}{1 - S_{wc} - S_{or}}\left(\frac{1 - S_w - S_{or}}{1 - S_{wc} - S_{or}}\right)^{n_o - 1} n_o k_{ro}(S_{wc}).$$

Before water breakthrough the cumulative recovered oil is equal to the volume of the injected fluid

$$PV_{inj} = N_p.$$

After water breakthrough, the amount of water injected is equal to

$$PV_{inj} = \frac{1}{\left.\frac{df_w}{dS_w}\right|_{S_{we}}}.$$

The derivative can be found as

$$\left.\frac{df_w}{dS_w}\right|_{S_{we}} = \frac{1-f_{we}}{S_{w,ave}-S_{we}}.$$

The average water saturation equation equals to

$$S_{w,ave} = S_{we} + (1-f_{we})PV_{inj}.$$

By subtracting the connate water saturation the produced oil can be calculated

$$N_p = S_{w,ave} - S_{wc} = (S_{we} - S_{wc}) + (1-f_w)PV_{inj}.$$

The recovery factor is calculated as

$$RF = \frac{N_p}{(1-S_{wc})}.$$

The concept of the average apparent viscosity should be introduced with the apparent (effective) viscosity equation

$$\lambda_r^{-1} = \frac{1}{\lambda_{ro}+\lambda_{rw}},$$

where λ_{ro} and λ_{rw} – relative mobilities of oil and water phases.

Then the average apparent viscosity is

$$\overline{\lambda^{-1}} = \frac{\int_0^L \lambda_r^{-1} dx}{\int_0^L dx}$$

and the total flow rate can be computed (in field units) as

$$q_t = \frac{1.127kA(p_i - p_p)}{\overline{\lambda^{-1}}L}.$$

Finally, the relationship between time and total flow rate is

$$t^{n+1} = t^n + \frac{2\left(PV_{inj}^{n+1} - PV_{inj}^{n}\right)PV}{(q_t^{n+1} + q_t^n)}.$$

APPENDIX D LINEAR WATERFLOOD AT CONSTANT RATE

The performance of a linear waterflood at constant injection rate is calculated based on the exact same equations listed in the Appendix B except the fact that rate $q_t = const.$ Then the pressure drop between the injector and producer (for oil field units) could be estimated as

$$\Delta p_{I-P} = \frac{\overline{\lambda^{-1}} L q_t}{1.127 k A}$$

and the relationship between time and displacement is

$$t = \frac{PV_{inj}}{q_t / A\phi L}.$$